EXPERIMENTAL LIMITATIONS IN THE KRAMERS-KRONIG TRANSFORMATION AND THE IMPORTANCE OF INTERFACE EFFECTS IN SPECTROSCOPIC ELLIPSOMETRY OF MoS_2 ON STO

TAN TU GUANG

NATIONAL UNIVERSITY OF SINGAPORE

2016

EXPERIMENTAL LIMITATIONS IN THE KRAMERS-KRONIG TRANSFORMATION AND THE IMPORTANCE OF INTERFACE EFFECTS IN SPECTROSCOPIC ELLIPSOMETRY OF MoS_2 ON STO

TAN Tu Guang

(*Department of Physics*)

A THESIS SUBMITTED

FOR THE DEGREE OF B.SC. (HONS.)

DEPARTMENT OF PHYSICS

NATIONAL UNIVERSITY OF SINGAPORE

2016

DECLARATION

I hereby declare that the thesis is my original work and it has been written by me in its entirety. I have duly acknowledged all the sources of information which have been used in the thesis.

This thesis has also not been submitted for any degree in any university previously.

TAN Tu Guang

1st April 2016

Acknowledgment

I would like to thank my supervisor Assistant Professor Andrivo Rusydi, and co-supervisor Dr Pranjal Gogoi, for patiently guiding me through this project. I would also like to thank my pizza buddies for the invaluable discussions: Jeremy Soh, Lai Jun Hao, Roslyn Ang, and especially Ng Yi'en for his crash course in Matlab.

And Thomas Edison for his extremely inspirational quote:

"I have not failed. I've just found 10,000 ways that won't work"

Contents

Abstract **vii**

1 Introduction **1**

1.1 Foreword 1

1.2 Motivation 1

1.3 Spectroscopic Ellipsometry 2

1.3.1 Principles of Spectroscopic Ellipsometry 2

1.3.2 ρ, Fresnel equations, and ϵ 3

1.3.3 The Lorentz Model 8

1.3.4 Spectroscopic Ellipsometry revisited 11

2 Methodology **13**

3 Results and Discussion **18**

3.1 Pseudo Dielectric Function of Bulk perovskite-type $SrTiO_3$ (100) . . 18

3.2 Pseudo Dielectric Function of MoS_2 on STO 19

3.3 Errors in Kramers-Kronig Transformation 20

3.3.1 Introduction to the Kramers-Kronig Transformation 20

3.3.2 Testing the transformation 21

3.3.3 1-Lorentzian toy model 23

3.3.4 Varying dω 27

3.3.5 Varying energy range 29

3.3.6 Bulk $SrTiO_3$ 32

3.3.7 Final remarks on the Kramers-Kronig transformation 35
3.4 Insufficiency of 3 layer optical model 36
3.4.1 Test fitting of substrate data 37
3.4.2 Unsuccessful fitting of ϵ of MoS_2 40

4 Conclusion **42**

5 Future Work **44**

Bibliography **46**

Appendix A Definition of optical constants used **52**

Appendix B ρ for the case of medium/substrate interface (Mathematica code) **54**

Appendix C ρ for the case of medium/thinfilm/substrate (Mathematica code) **57**

Appendix D Hamiltonian for free field of Light **62**

Appendix E Error analysis for Kramers-Kronig transformation (Matlab code) **66**

E.1 100 data points, 13.2eV range 67
E.2 Comparing 6.5eV range to 20eV range with constant data point density of $\approx$ 150 points per eV 69
E.3 Comparing 50 data points to 1000 data points, 13.2eV range 72

Appendix F Manual fitting of the Lorentz model to experimental data (Matlab code) **76**

Appendix G Analysis of fitting attempts for MoS_2 bilayer on STO using 3 layer optical model and 3-Lorentzian model **87**

Abstract

Spectroscopic ellipsometry is a non-destructive, highly sensitive characterization technique that can be used to investigate interface effects. However, data treatment is highly non-trivial. While this makes it a difficult technique to use, it can unambiguously reveal the presence of surface roughness, interface effects, etc. In this report, we examine 2 textbook approaches to extracting the complex dielectric function of MoS_2 from a sample of bilayer MoS_2 on $SrTiO_3$ substrate. More specifically, we examine the errors introduced during the manual application of the Kramers-Kronig transformation, which is a common constraint used in solving the inverse ellipsometry problem. Optical modeling is also another integral part of ellipsometry, and we examine the feasibility of using a 3-layer optical model for studying MoS_2 on $SrTiO_3$. The errors introduced when performing the Kramers-Kronig transformation on typical experimental results are found to be highly non-trivial, and the 3-layer optical model was found to be unsuitable due to strong interface effects in our sample.

Chapter 1

Introduction

1.1 Foreword

This report documents one student's journey to understand spectroscopic ellipsometry, and focuses on extracting useful information out of the raw Ψ/Δ data. It will examine the theory behind how ellipsometry works and the ideas behind the subsequent treatment of data. As example of the extraction of the complex dielectric constants of thin-film MoS_2 from a sample of thin-film MoS_2 on $SrTiO_3$ substrate is provided, but no in-depth examination of said constants will be made. Similarly, the experimental data were taken as they were and no in-depth examination of the samples themselves will be made.

1.2 Motivation

As miniaturization proceeds, silicon based Metal Oxide Semiconductor Field Effect Transistors (MOSFETs) face a limit in the onset of thermal and quantum effects [1, 2]. The search for alternatives had led to novel materials such as Graphene [3, 4]. However, the lack of an intrinsic band gap and high costs of production pose many practical problems [5, 6]. Subsequent research has revealed Transition Metal Dichalcogenides (TMDCs) to share many desirable properties due to their layered structures [7]. One such material is Molybdenum Disulphide (MoS_2). MoS_2 is of

particular interest due to the similarity of its band gap to typical semiconductors [8].

However, the precise and accurate characterization of a thin film's material properties is a non-trivial matter [9]. The Singapore Synchrotron Light Source (SSLS) [10] opens up spectroscopic ellipsometry as one of the options available to us [11]. Non-destructive, versatile and extremely sensitive, spectroscopic ellipsometry is an excellent method for investigating the optical and electronic properties of materials and interface effects [12]. Prior to the prevalence of ellipsometry, reflectivity measurements were often done to investigate optical properties, but the lack of phase information encourages the use of the Kramers-Kronig relations [13, 14, 15]. Even when treating ellipsometry data, the relations are sometimes used as a constraint to solve the inverse ellipsometry problem [16]. The errors introduced when applying the transformation to typical experimental data are suspected to be non-trivial, and will be investigated in this report.

The alternative to solving the inverse ellipsometry problem is to use an optical model and dielectric function model to fit the experimental data [12]. Performing spectroscopic ellipsometry on a thin-film MoS_2 on STO substrate suggests the use of an air-film-substrate (3 layer) optical model. The validity of this model in investigating MoS_2 on STO will be tested in this report.

1.3 Spectroscopic Ellipsometry

1.3.1 Principles of Spectroscopic Ellipsometry

Ellipsometry is an optical characterization technique that measures the changes in light polarization after reflecting off a sample. Fig. 1.1 provides an idea of the measurement principle of ellipsometry.

Due to the optical properties of the sample, the s and p polarizations of light will often have different responses as they reflect off the sample, leading to an elliptical

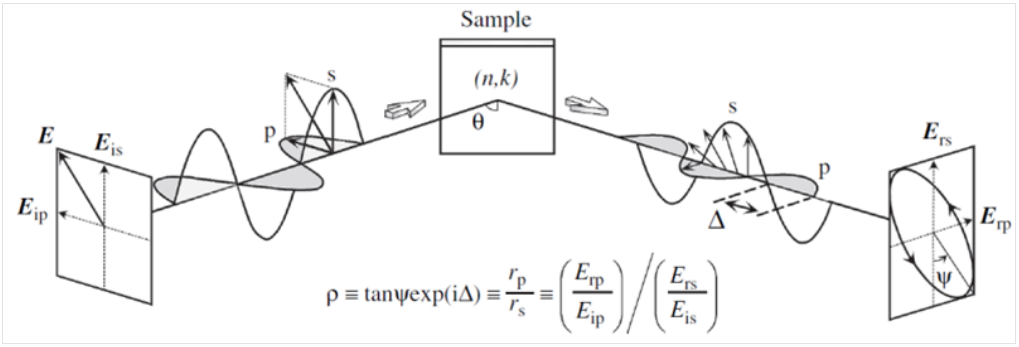

Fig. 1.1. measurement principle of ellipsometry [12]

polarization [1]. Measurement results are recorded as 2 values, the amplitude ratio (Ψ) and phase difference (Δ), which quantify these differences between the 2 polarizations. This can be done for different wavelengths of light to obtain the optical response of the material over a spectral range in a technique called spectroscopic ellipsometry.

After shining light of different wavelengths on the sample and tabulating the corresponding Ψ and Δ values, the physical meaning of the data will not be immediately apparent. An optical model is required to proceed further.

1.3.2 ρ, Fresnel equations, and ϵ

We examine Fig. 1.1 for its equation:

$$\rho \equiv tan(\Psi)exp(i\Delta) \equiv \frac{r_p}{r_s} \equiv \frac{E_{rp}}{E_{ip}} / \frac{E_{rs}}{E_{is}} \tag{1.1}$$

By solving the boundary conditions for light at an interface, one can derive the Fresnel equations that relate the reflected electric field to the incident field [17]. These give us (1.2) and (1.3), where the subscripts i and t denote incident and transmitted parameter respectively [12].

$$r_p = \frac{N_t cos(\theta_i) - N_i cos(\theta_t)}{N_t cos(\theta_i) + N_i cos(\theta_t)} \tag{1.2}$$

[1] hence the name ☺

$$r_s = \frac{N_i cos(\theta_i) - N_t cos(\theta_t)}{N_i cos(\theta_i) + N_t cos(\theta_t)} \tag{1.3}$$

Bulk sample

The information we have thus far is sufficient to be applied to the ellipsometry of a bulk sample. In such a situation, (1.2) and (1.3) can be directly applied as illustrated in Fig. 1.2.

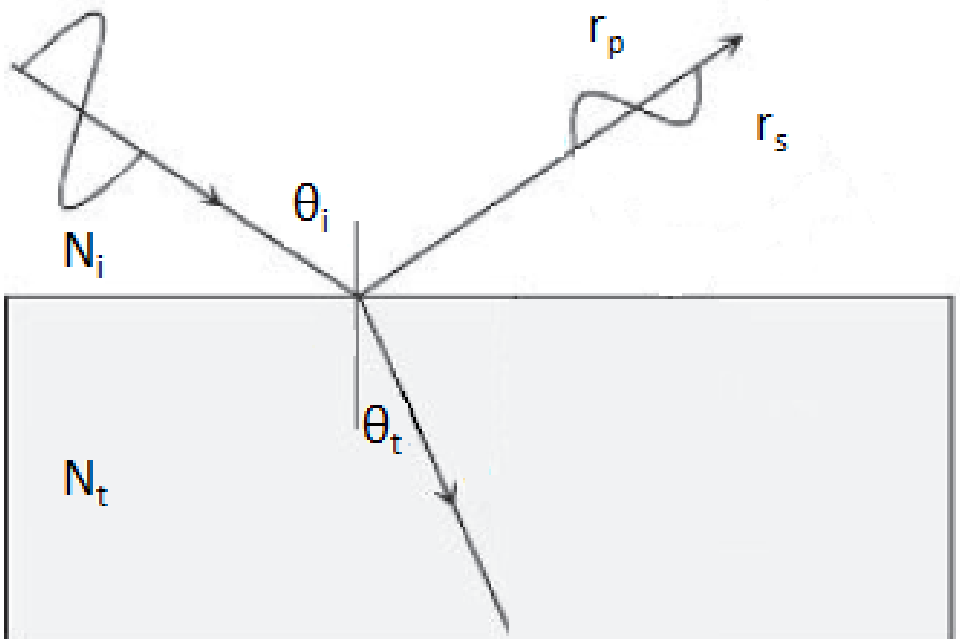

Fig. 1.2. Reflection of light off a bulk sample

Using (1.1), (1.2) and (1.3), we can obtain an expression for ϵ as follows[2], noting that the material property N_t is related to ϵ_t by the definition $N^2 \equiv \epsilon$.

$$\epsilon_t = \frac{(1 + \rho^2 + 2\rho cos(2\theta_i))\epsilon_i tan(\theta_i)^2}{(1+\rho)^2} \tag{1.4}$$

In this form, ϵ_t is expected to be calculated from experimental values of ρ, and is differentiated from the material's true complex dielectric function by the notation $< \epsilon >$. $< \epsilon >$ is referred to as the Pseudo Dielectric Function (PDF). In the situation where the sample really is an infinitely thick bulk material with a perfectly smooth

[2]See Appendix B

top surface, the pseudo dielectric function is a good approximation to the material's true dielectric function.

Thin film on substrate

Expanding upon Fig. 1.2, we can add another layer to model the situation for a thin film on substrate sample. We begin with an air-film-substrate model (3 layer optical model). N_0 (air) is set to be completely real with $n = 1$ and $k = 0$ to simplify further calculations.

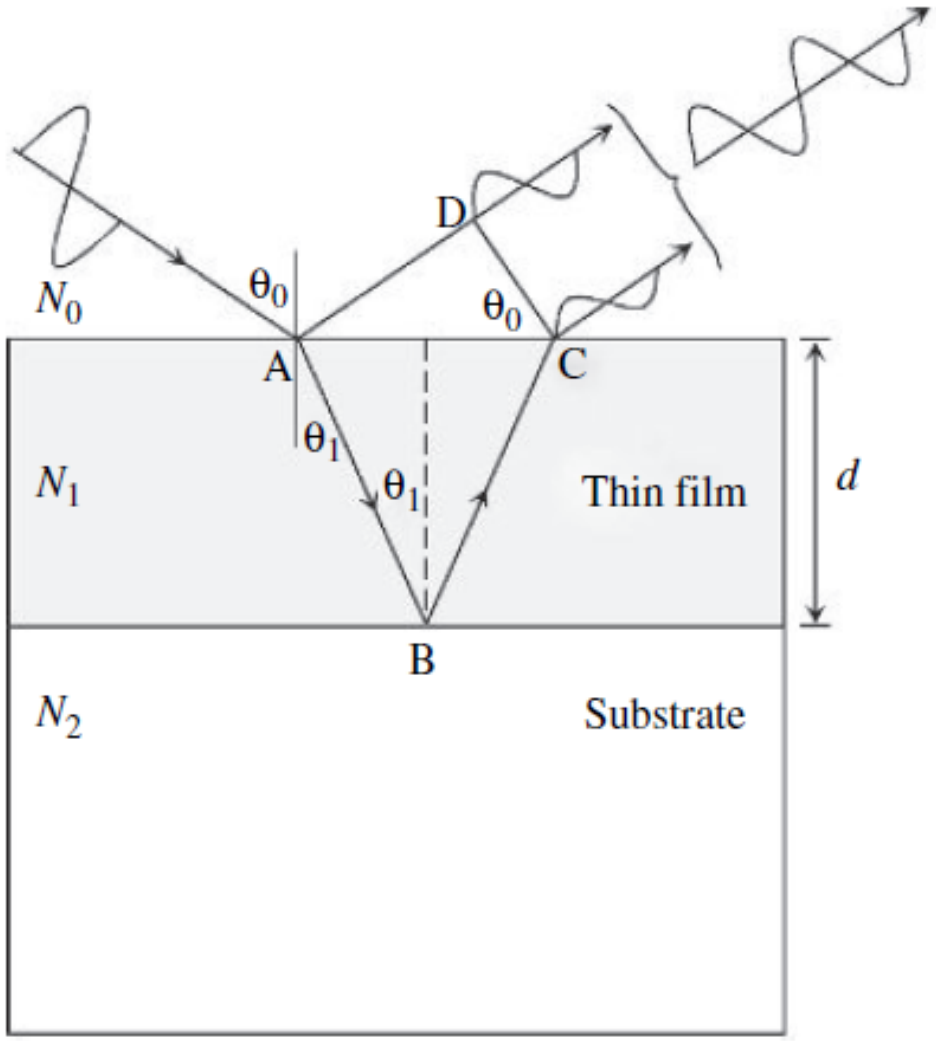

Fig. 1.3. 'Toy model' of air-film-substrate [12]

We first consider the air-film (subscript 01) interface. Indices j and k can be introduced to (1.2) and (1.3) to give us:

$$r_{p,jk} = \frac{N_k cos\theta_j - N_j cos\theta_k}{N_k cos\theta_j + N_j cos\theta_k} \tag{1.5}$$

and

$$r_{s,jk} = \frac{N_j cos\theta_j - N_k cos\theta_k}{N_j cos\theta_j + N_k cos\theta_k} \tag{1.6}$$

The equations share the same form at the film-substrate (subscript 12) interface. The equations for transmission coefficients are

$$t_{p,jk} = \frac{2N_j cos\theta_j}{N_k cos\theta_j + N_j cos\theta_k} \tag{1.7}$$

$$t_{s,jk} = \frac{2N_j cos\theta_j}{N_j cos\theta_j + N_k cos\theta_k} \tag{1.8}$$

Rays transmitted into the substrate are ignored since we assumed a thick substrate (i.e. they do not get reflected back to the detector).

Our experimental results ρ measure $r_{p,total}/r_{s,total}$, the expression of which can be obtained through an exercise in geometry (Fig. 1.3). The phase difference between the two reflected rays at point C and D is given by

$$\alpha = \frac{4\pi d N_1 cos\theta_1}{\lambda} \tag{1.9}$$

Notice that the ray AB-BC passes through the film twice. By physical insight and foresight, we define the film phase thickness β by

$$\beta \equiv \frac{\alpha}{2} = \frac{2\pi d N_1 cos\theta_1}{\lambda} \tag{1.10}$$

We now extend the situation to include all higher order rays (Fig. 1.4). We can express any wave for r_{01} with $exp(i(\omega t - kx + \delta))$ [3]. The next higher order wave will then acquire an extra path difference of 2β, which can be expressed as a factor

[3]The Optics convention is used in this project. See Appendix A

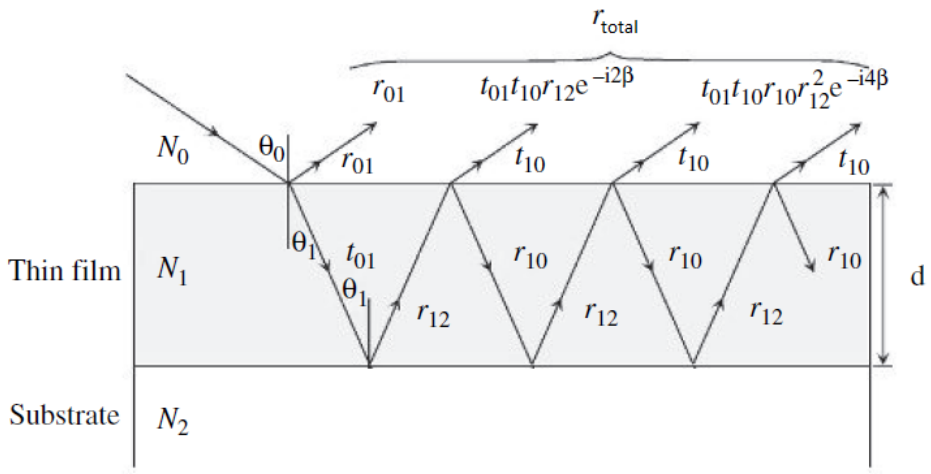

Fig. 1.4. Optical model of air-film-substrate [12]

of $exp(-2i\beta)$. Multiplying the amplitude coefficients at each interface, we get

$$r'_{01} = t_{01}r_{01}exp(-2i\beta)t_{10} \tag{1.11}$$

Thus, we see that the summation to obtain r_{total} is a geometric series, with an additional factor of $t_{01}exp(-2i\beta)t_{10}$ for the next higher order ray. The series is solved to give

$$r_{total} = r_{01} + \frac{t_{01}t_{10}r_{12}exp(-2i\beta)}{1 - r_{10}r_{12}exp(-2i\beta)} \tag{1.12}$$

From equations 1.5 and 1.6, we note that $r_{01} = -r_{10}$, and from equations 1.7 and 1.8, we note that $t_{01}t_{10} = 1 - r_{01}^2$. Thus, we obtain

$$r_{total} = \frac{r_{01} + r_{12}exp(-2i\beta)}{1 + r_{01}r_{12}exp(-2i\beta)} \tag{1.13}$$

This gives us the measured r_p and r_s as follows:

$$r_{total,p} = \frac{r_{p,01} + r_{p,12}exp(-2i\beta)}{1 + r_{p,01}r_{p,12}exp(-2i\beta)} \tag{1.14}$$

$$r_{total,s} = \frac{r_{s,01} + r_{s,12}exp(-2i\beta)}{1 + r_{s,01}r_{s,12}exp(-2i\beta)} \tag{1.15}$$

With this, we get the expression for ρ:

$$\rho = \frac{r_{p,01} + r_{p,12}exp(-2i\beta)}{1 + r_{p,01}r_{p,12}exp(-2i\beta)} \div \frac{r_{s,01} + r_{s,12}exp(-2i\beta)}{1 + r_{s,01}r_{s,12}exp(-2i\beta)} \tag{1.16}$$

Now, we insert the expressions for $r_{p,jk}$ and $r_{s,jk}$ (equations 1.5 and 1.6). We set the complex refractive index of air (N_0) to be 1, and using Snell's Law ($N_j sin\theta_j = N_k sin\theta_k$) to obtain the expression for $cos\theta_k$ ($cos\theta_k = \sqrt{1 - (\frac{N_j}{N_k} sin\theta_j)^2}$), we get [4]:

$$\rho = \rho(d, N_1, N_2, \theta_0) \tag{1.17}$$

which is a messy equation but essentially a function of the 4 listed variables.

Here, the two experimental quantities Ψ and Δ provide the quantity ρ itself. Incident angle θ_0 is a controlled experimental parameter, and the complex refractive index of the substrate N_2 is assumed to be known through prior experiments. This leaves 3 unknowns in the form of thin film thickness d, and thin film complex refractive index $Re(N_1)$ and $Im(N_1)$.

If the complex refractive indices of the materials are known, it is possible to obtain an analytical solution for the thickness of the film [18]. This inspires the Inverse Ellipsometry Problem: if the thickness is known via other characterization methods, or if a second set of data is taken, is it possible to solve for N_1 analytically, especially with the Kramers-Kronig constraint applied? An analysis of this method will be made and presented in Section 3.3.

1.3.3 The Lorentz Model

The Lorentz model is a purely classical model that assumes that the dipoles in matter can be modeled as an electron oscillating about a positively charged nucleus as shown in Fig. 1.5.

As light (electromagnetic waves) hit this dipole, the alternating electric field will provide a force in the x-direction. This E field can be described by a simple

[4] See Appendix C

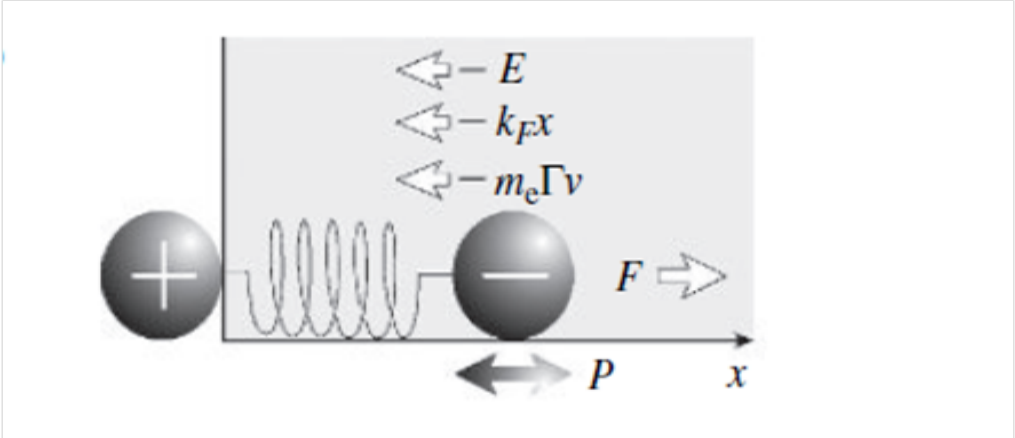

Fig. 1.5. The Lorentz model [12]

oscillating function (1.18).

$$E = E_0 exp(i\omega t) \tag{1.18}$$

Taking the massive nucleus as the reference point, we expect the electron to move in the same direction. The model assumes that the restoring force obeys Hooke's Law in that it is linearly proportional to the distance from its equilibrium point (the nucleus), with the proportionality constant ω_0 being its natural frequency. The model further includes a drag term which is proportional to the mass and velocity of the electron, with the constant Γ describing the "viscosity" of the fluid in which the electron is moving in. With these 3 forces describing the movement of the bound electron, we can quantify the "stretching" of the dipole using Newton's second law (F=ma), as shown in (1.19).

$$m_e \frac{d^2x}{dt^2} = -m_e \Gamma \frac{dx}{dt} - m_e \omega_0^2 x - eE_0 exp(i\omega t) \tag{1.19}$$

The solution to (1.19) is:

$$x(t) = a exp(i\omega t) \tag{1.20}$$

where the factor a is given by

$$a = -\frac{eE_0}{m_e} \frac{1}{(\omega^2 - \omega_0^2) + i\Gamma\omega} \tag{1.21}$$

We know that the total polarization is given by (1.22) which is essentially the number of electrons (N_e) multiplied by charge times distance (definition of dipole moment [17]).

$$P = -eN_e x(t) \tag{1.22}$$

We also know that the dielectric constant ϵ is given by (1.23) [17].

$$\epsilon = 1 + \frac{P}{\epsilon_0 E} \tag{1.23}$$

Substituting the expressions for E (1.18) and P (1.22) into the above expression for ϵ (with the $x(t)$ in P given by (1.20)), we get (1.24)

$$\epsilon = 1 + \frac{e^2 E_0}{\epsilon_0 m_e} \frac{1}{(\omega^2 - \omega_0^2) + i\Gamma\omega} \tag{1.24}$$

which is in general complex. A simple conjugation operation splits the expression into its real and complex parts with $\epsilon = \epsilon_1 - i\epsilon_2$:

$$\epsilon_1 = 1 + \frac{e^2 E_0}{\epsilon_0 m_e} \frac{(\omega^2 - \omega_0^2)}{(\omega^2 - \omega_0^2)^2 + \Gamma^2\omega^2} \tag{1.25}$$

$$\epsilon_2 = \frac{e^2 E_0}{\epsilon_0 m_e} \frac{\Gamma\omega}{(\omega^2 - \omega_0^2)^2 + \Gamma^2\omega^2} \tag{1.26}$$

The above is plotted in Fig. 1.6 with dummy values of $\omega_0 = 6.08 \times 10^{15}$ rad/s (4 eV) and $\Gamma = 1.2 \times 10^{15}$ rad/s.

What this essentially means is that the optical response of a material can be modeled by a collection of simple harmonic oscillators[5]. Thus, any material can be described by (1.27) and (1.28) where A_k describes the different relative amplitudes of the oscillators.

$$\epsilon_1 = 1 + \sum_k \frac{A_k e^2 E_0}{\epsilon_0 m_e} \frac{(\omega^2 - \omega_{0,k}^2)}{(\omega^2 - \omega_{0,k}^2)^2 + \Gamma_k^2\omega^2} \tag{1.27}$$

[5]Remarkably, this result has been verified by quantum optics even though this classical model was developed over a century ago. See Appendix D for the quantum mechanical confirmation of this result.

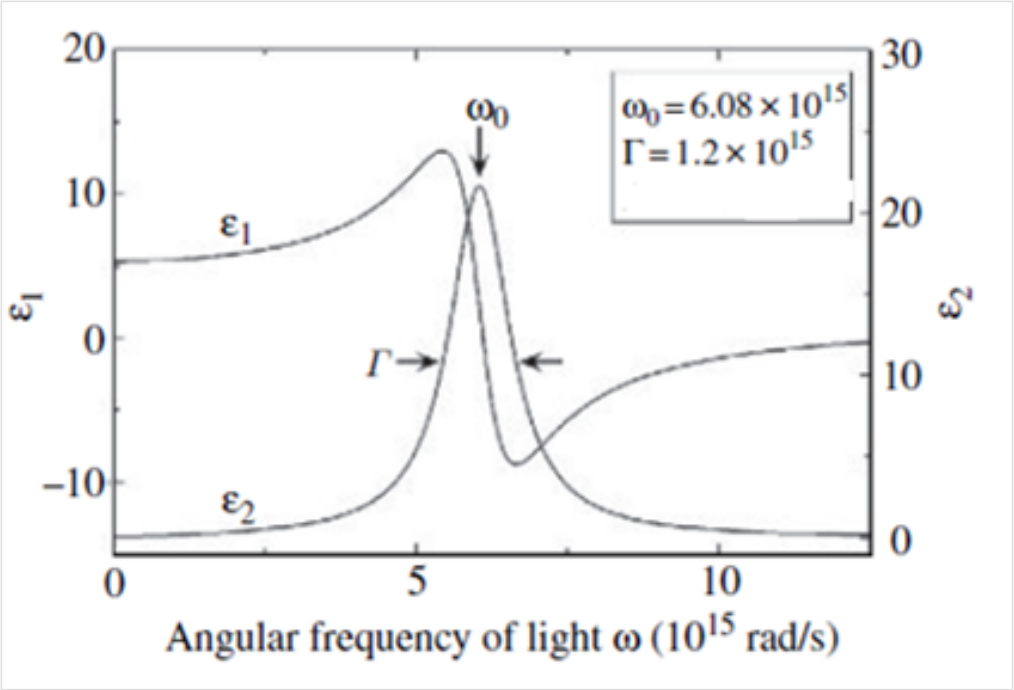

Fig. 1.6. ϵ from the Lorentz model [12]

$$\epsilon_2 = \sum_k \frac{A_k e^2 E_0}{\epsilon_0 m_e} \frac{\Gamma_k \omega}{(\omega^2 - \omega_{0,k}^2)^2 + \Gamma_k^2 \omega^2} \tag{1.28}$$

The Lorentz model thus allows us to analyze the optical properties of a material component by component, and identify the type of each oscillator through subsequent analysis.

1.3.4 Spectroscopic Ellipsometry revisited

We are now armed with sufficient knowledge to appreciate the full process. Suppose we have material A, whose optical properties can be modeled by the Lorentz model. Light is reflected off material A and is now elliptically polarized. This reflected light is detected by the ellipsometer. The relative amplitude between the s- and p-polarized light is recorded as Ψ, and the relative displacement recorded as Δ, as shown in Fig. 1.1. The Ψ and Δ values are related to the material by (1.1). The analytical form of the Fresnel reflection coefficients r_p and r_s are known. These can be further manipulated to give an expression for the complex dielectric constant ϵ if we accept that r_p and r_s can be modeled from the Lorentz model. Thus, we are now able to relate Ψ and Δ to ϵ, and ϵ provides all information on the optical

properties of the material.

Suppose we now have material B. All of the above applies similarly. However, if we consider a thin film of material A on top of a substrate of material B, there is an additional effect to consider. If the film of material A is thin enough, light may be able to pass in through material A, reflect at the material A/B interface, pass out through material A again, and exit the sample to interfere with the light that is reflected at the air/material A interface. The condition for this effect to be significant is that the light intensity is reduced to e^{-1} (about 37%) of its incident intensity, and the thickness at which this occurs is defined as the penetration depth (d_p) [17, 12] [6]. The analytical form of d_p is given by $1/\alpha$, where α is given by (1.29). In other words, if our film of material A is thinner than d_p, these interference effects at the material A/material B interface must be considered. If the layer of material A is much thicker than d_p, however, we can completely ignore material B and simplify our analysis as if we are performing bulk ellipsometry on material A. Due to the high sensitivity of ellipsometry measurements, these interference effects can still be detected at up to $5d_p$ [19]. These interference effects allow us to determine the thickness of the film, but also complicate our calculations. Our sample has an estimated thickness of about 1.5 nm for MoS_2 bilayer [20, 21], so interference effects are expected to be significant[7].

$$\alpha = \frac{4\pi k}{\lambda} \tag{1.29}$$

[6] It may be useful to note here that some literature quote the skin depth d_e which is related to the decay of the electric field rather than the intensity, and is related by $d_e = 2d_p$ due to $I = |E|^2$

[7] A quick estimate using k=1 (typical values are 10^{-2}), $\lambda = 10^{-7}$ gives $d_p \approx 10^{-8}$m, which is an order of magnitude higher than our estimated thickness

Chapter 2

Methodology

Spectroscopic ellipsometry was performed on 2 samples at 300 K at the SSLS [10]:

- (100) face of bulk Perovskite-type $SrTiO_3$
- Bilayer MoS_2 deposited on (100) face of bulk Perovskite-type $SrTiO_3$

The end goal is to extract ϵ from the Ψ and Δ experimental data of the 2 samples. The raw experimental data is shown in Fig. 2.1 and Fig. 2.2.

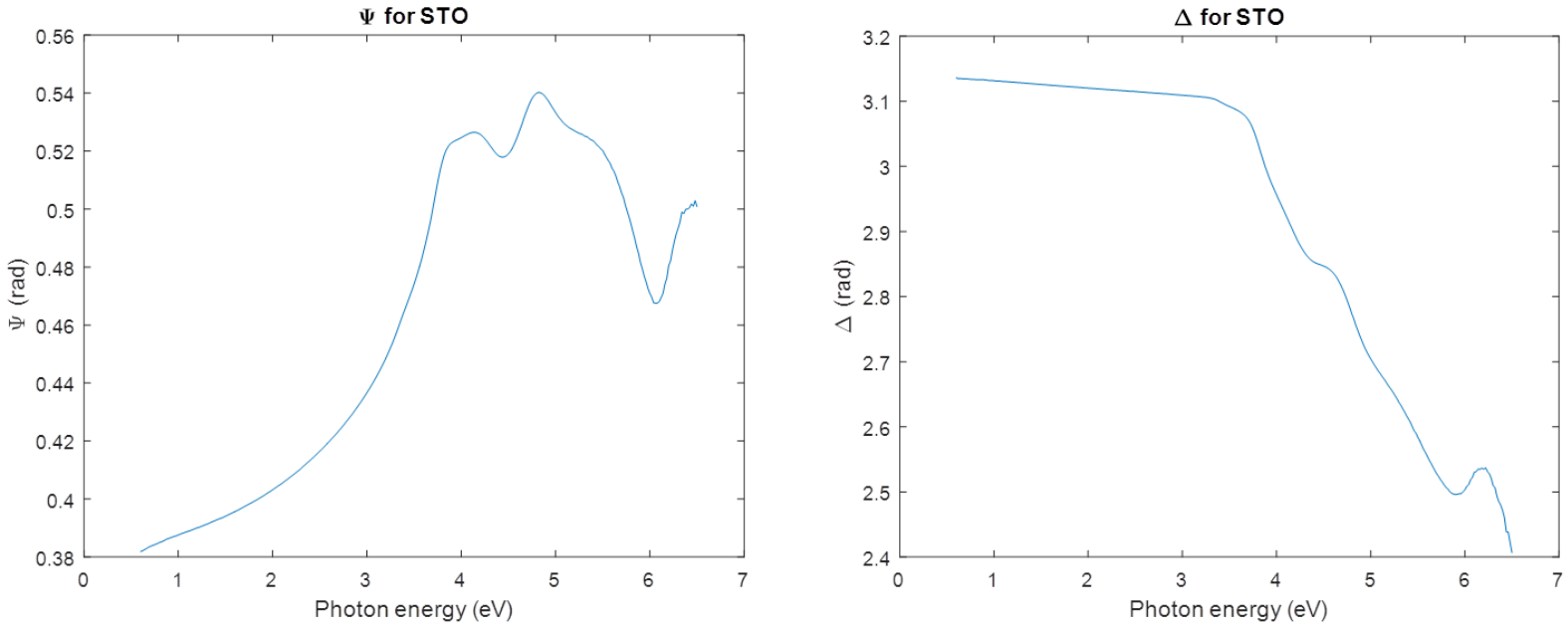

Fig. 2.1. Raw experimental data for STO, 50 degree incident angle

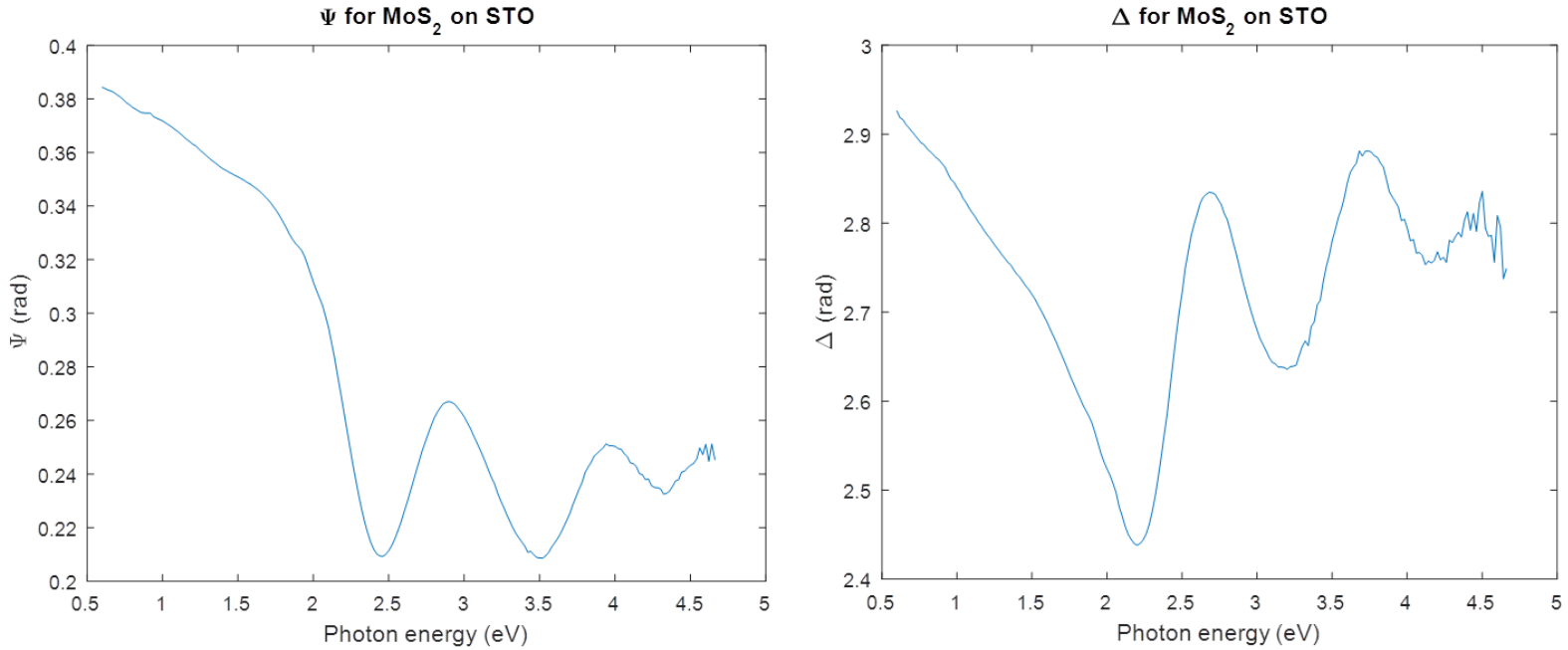

Fig. 2.2. Raw experimental data for MoS_2 on STO, 50 degree incident angle

Now, we know how the interference effects will behave (Section 1.3.2), and we have the substrate data (Fig. 2.1). However, due to the complex nature of the interference effects no analytical method of extracting the optical constants of MoS_2 from the data exists. Thus, the following 2 methods are examined:

1. Kramers-Kronig constrained numerical solution to the inverse ellipsometry problem

2. Lorentzian fitting using a 3-Lorentzian model

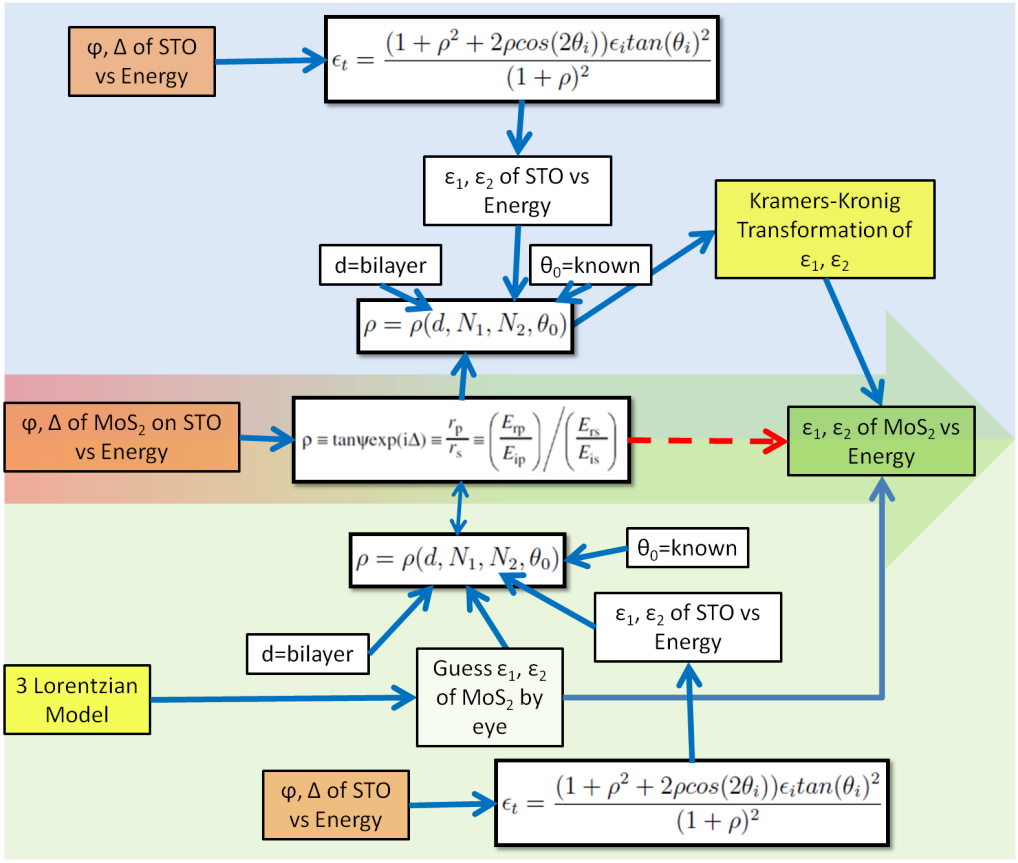

Fig. 2.3. Schematic diagram of the methodology. Red denotes raw data, green denotes desired result, and yellow denotes the step that is examined in this report. The top half represents the inverse ellipsometry problem while the bottom half represents Lorentzian fitting.

A schematic diagram of the methodology is shown in Fig. 2.3. For method 1, Ψ/Δ provides the experimental value ρ at each incident photon energy. The analytical form of ρ as derived in Appendix C is complicated but ultimately an equation of 4 independent variables: film thickness d, film complex dielectric constant N_1,

substrate complex dielectric constant N_2, and incident photon angle θ_0. N_1 can easily be obtained directly from the experimental Ψ/Δ values of STO (equation (1.4)). θ_0 is an experimental parameter and known. d can be measured via other experimental techniques such as atomic force microscopy [20], or even measured in-situ via electron diffraction [9]. In any case, we can assume d to be known (this assumption can always be relaxed later). This leaves N_1 as the only unknown. Since this is a complex value, we can then further apply the Kramers-Kronig constraint to reduce it to only 1 independent unknown (either the real or the complex part), which can then be solved numerically. Indeed, this method is widely employed in analyzing reflectivity and ellipsometry data [12, 16, 22].

Due to the large role that the Kramers-Kronig transformation plays in this method, Section 3.3 will be devoted to analyzing the errors that may be introduced during the transformation. This will be done using Matlab (see Appendix E).

For method 2, a model for N_1 is created using 3 Lorentzians, based on (1.27) and (1.28). The parameters ω_0, Γ, and relative amplitude A for each of the 3 Lorentzians (total of 9 parameters) are entered by hand. ρ is then calculated and compared to the experimental $\rho(\Psi, \Delta)$. The 9 parameters are then readjusted to obtain a better fit between the fitted ρ and the experimental ρ. These will be done using Matlab (see Appendix F). The figure of merit for this "goodness of fit" is quantized by different methods in different literature [23, 24, 25]. Possible ways include minimizing the mean-square-error (MSE) or the Chi-square. Indeed, the best way to quantify fitting errors remains a formidable research area by itself and is outside the scope of this project. For this project, the fitting will be done by eye, as more study is required to choose an appropriate way to quantify the goodness of fit.

For both methods, the expression for $\rho(d, N_1, N_2, \theta_0)$ was calculated from the air-film-substrate (3 layer) optical model using Mathematica (see Appendix B and Appendix C), and the resulting expression directly exported into Matlab for subsequent calculations.

Chapter 3

Results and Discussion

3.1 Pseudo Dielectric Function of Bulk perovskite-type $SrTiO_3$ (100)

As shown in Appendix B, the pseudo dielectric function calculation (equation (1.4)) for bulk ellipsometry allows us to directly obtain ϵ (Fig. 3.1) from the experimental data Ψ and Δ (Fig. 2.1).

Assuming the pseudo dielectric function is a good approximation for the true complex dielectric function, this knowledge is integral and sufficient for subsequent treatment of our MoS_2 on STO data, so no further analysis needs to be performed on STO at this juncture.

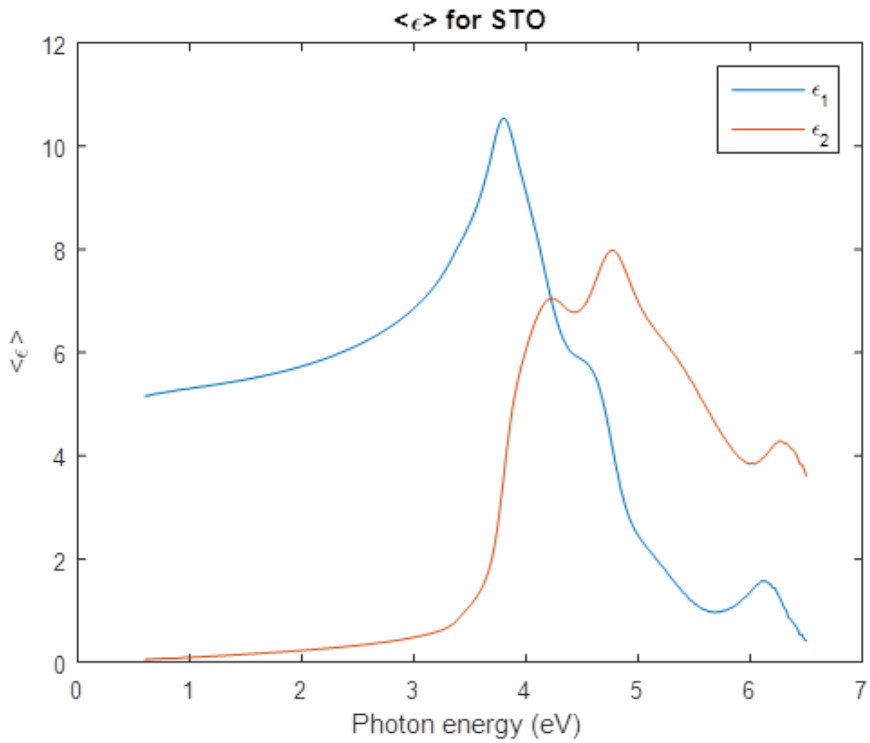

Fig. 3.1. $< \epsilon >$ for STO

3.2 Pseudo Dielectric Function of MoS_2 on STO

If we treat our MoS_2 on STO sample as a whole and think of it as a single bulk material, we can use a 2 layer optical model (air-bulk) to find the pseudo dielectric function of the sample, in a way similar to that outlined in Section 3.1. The PDF of this sample is shown in Fig. 3.2 together with that of STO.

As can be seen from Fig. 3.2, the de-convolution of MoS_2 optical properties is non-trivial even with knowledge of substrate data, due to interference effects. To gain any physical insight, we need a 3 layer optical model (Section 1.3.2) at the very least. As outlined in Chapter 2, we can proceed either by solving the inverse ellipsometry problem, or by fitting. The next section examines the Kramers-Kronig transformation, an often used constraint in the inverse ellipsometry problem.

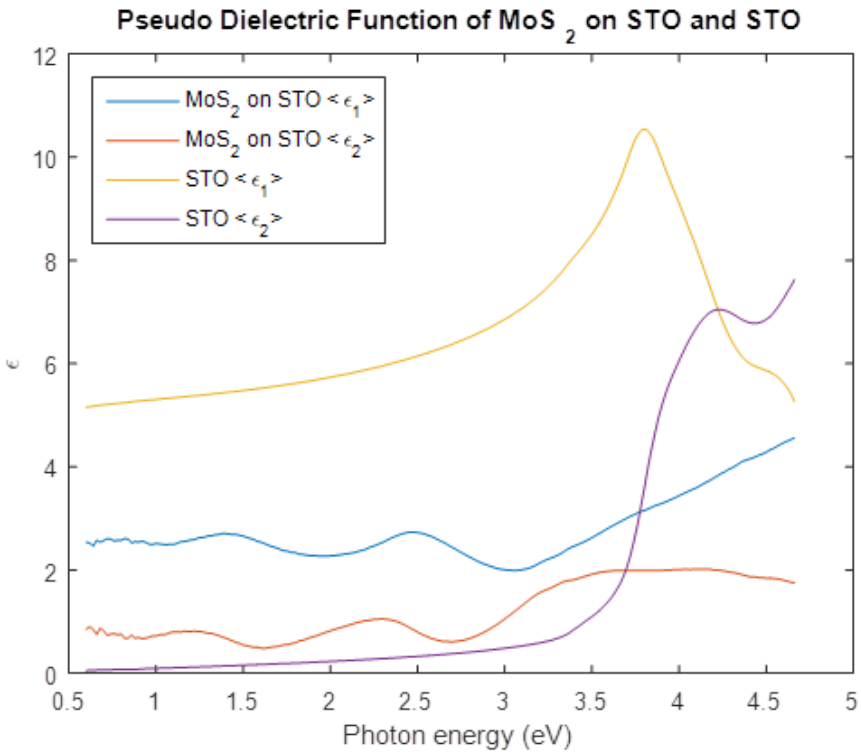

Fig. 3.2. De-convolution of MoS_2 optical properties is non-trivial even with knowledge of substrate data

3.3 Errors in Kramers-Kronig Transformation

3.3.1 Introduction to the Kramers-Kronig Transformation

As is evident from the Lorentz model (Section 1.3.3), ϵ_1 and ϵ_2 are not independent. The relationship between the 2 quantities is given by [12]:

$$\epsilon_1(\omega) = 1 + \frac{2}{\pi} P \int_0^\infty \frac{\omega' \epsilon_2(\omega')}{\omega'^2 - \omega^2} d\omega' \tag{3.1}$$

$$\epsilon_2(\omega) = -\frac{2\omega}{\pi} P \int_0^\infty \frac{\epsilon_1(\omega') - 1}{\omega'^2 - \omega^2} d\omega' \tag{3.2}$$

where $P \int_0^\infty d\omega'$ is simply shorthand for

$$P \int_0^\infty d\omega' \equiv \lim_{\delta \to 0} \left(\int_0^{\omega - \delta} d\omega' + \int_{\omega + \delta}^\infty d\omega' \right) \tag{3.3}$$

Mathematically, the relations arise from Cauchy's theorem for integrals on the complex plane. Physically, the condition that the function must be analytic arises

from causality [26, 27]. Consider the following example [28]: let's say that I am in a completely dark room. Deciding to turn on the lights in the near future, I know that the electric field of the room as a function of time contains a step function. I can perform a Fourier transform to obtain the electric field as a function of frequency instead, and realise that the reason the room is dark right now is not that there is no light, but rather that all the frequencies cancel each other out to give a sum of zero. This implies that I could wear a pair of sunglasses to block out some wavelengths (so that final sum is now no longer zero) and I will be able to see in a dark room as long as there was/will be light in the room any time in the past or future! This is obviously wrong and is due to the fact that a simple Fourier transform does not take causality into account.

For our purpose, the Kramers-Kronig transformation is of interest because it allows us to reduce the 2 unknowns ϵ_1 and ϵ_2 into 1 unknown, thereby allowing us to solve for them more easily. However, the equations (3.1) and (3.2) contain $\int$, ∞, and $d\omega'$, all of which are physically unattainable. This chapter examines the errors introduced from performing such a transformation.

3.3.2 Testing the transformation

Matlab was used to perform all analysis required in this chapter (Appendix E). A set of "perfect" ϵ_1 and ϵ_2 as a function of photon energy was created (Fig. 3.3) using the Lorentz model (1.25) and (1.26), with the amplitude coefficient (A) set arbitrarily to be equal to $\frac{e^2 E_0}{\epsilon_0 m_e} = 1.6 * 10^{32}\ (rad/s)^2$. ω_0 and Γ are also set arbitrarily at $6.08 * 10^{15}\ rad/s$ and $1.2 * 10^{15}\ rad/s$ respectively.

Next, the Kramers-Kronig transformation was used to obtain the transformed ϵ_2 from the analytical ϵ_1, and the transformed ϵ_1 from the analytical ϵ_2 (Fig. 3.4).

Finally, to compare the results, the absolute and percentage error is taken at each data point and the errors plotted out.

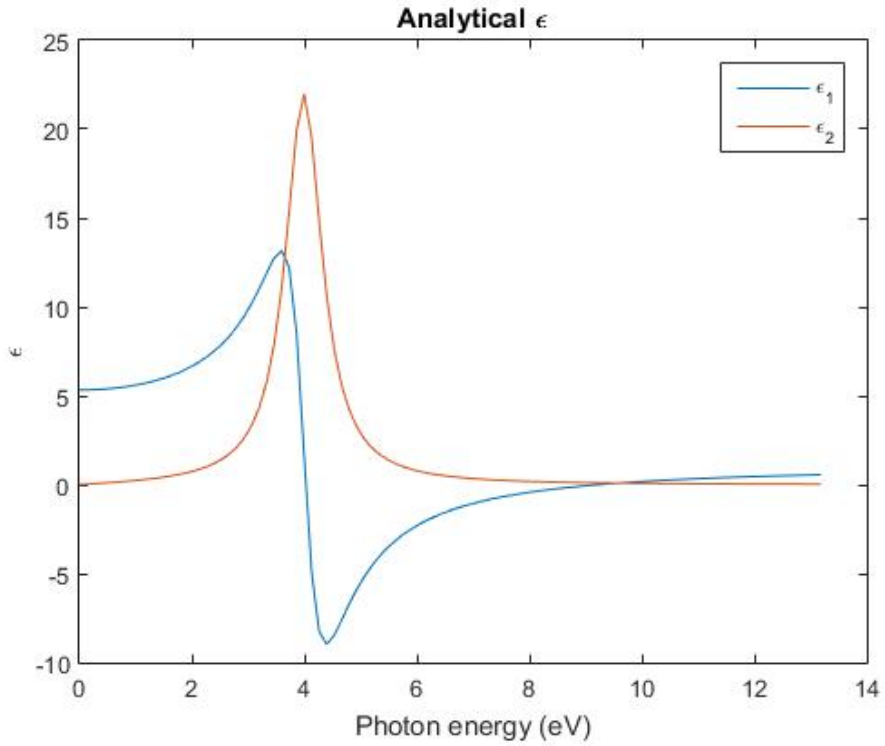

Fig. 3.3. "Perfect" ϵ generated from the Lorentz model

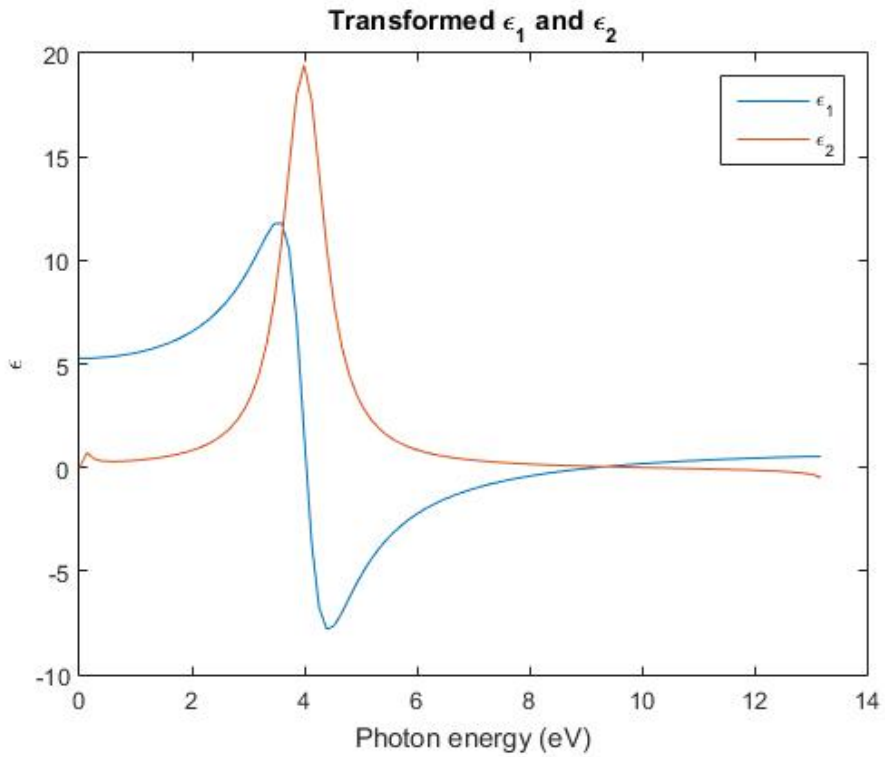

Fig. 3.4. Transformed ϵ from the Kramers-Kronig relations

3.3.3 1-Lorentzian toy model

The transformed ϵ and the analytical ϵ can be plotted together to see the difference by eye (Fig. 3.5 and Fig. 3.6).

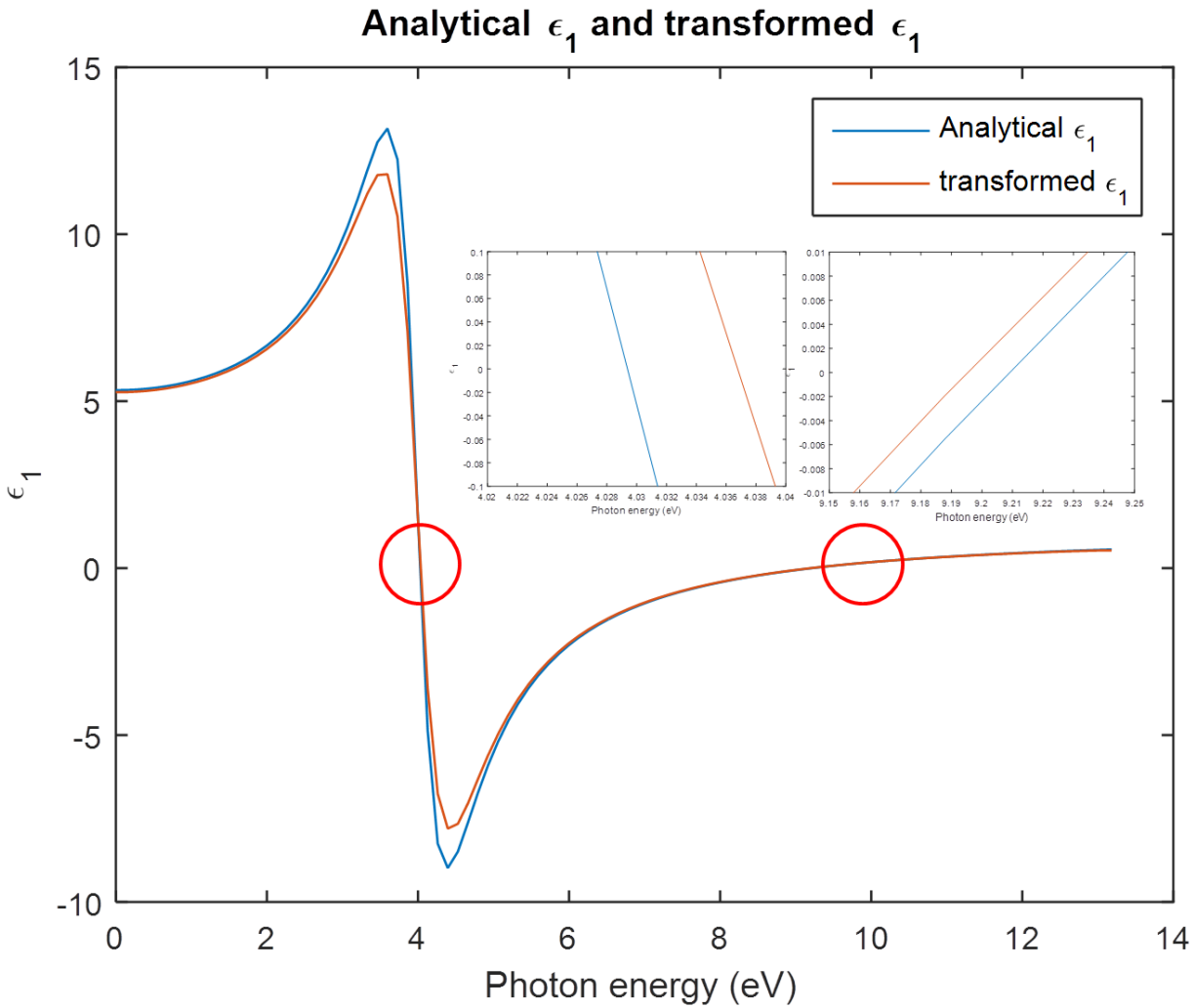

Fig. 3.5. Comparison of transformed ϵ_1 with analytical ϵ_1 (Insert: Magnified view of ϵ at the zero crossing)

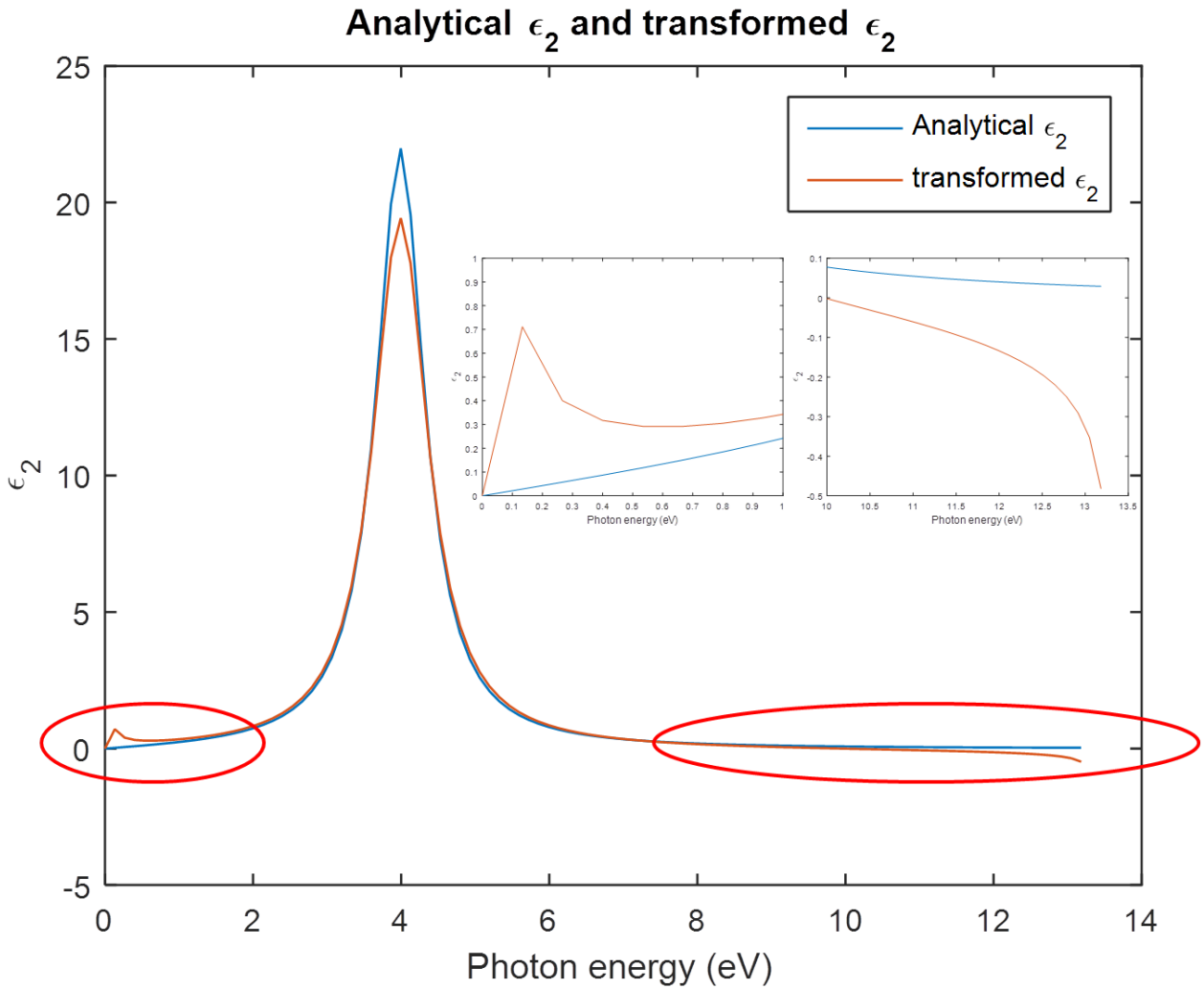

Fig. 3.6. Comparison of transformed ϵ_2 with analytical ϵ_2 (Insert: Magnified view of ϵ at range edges)

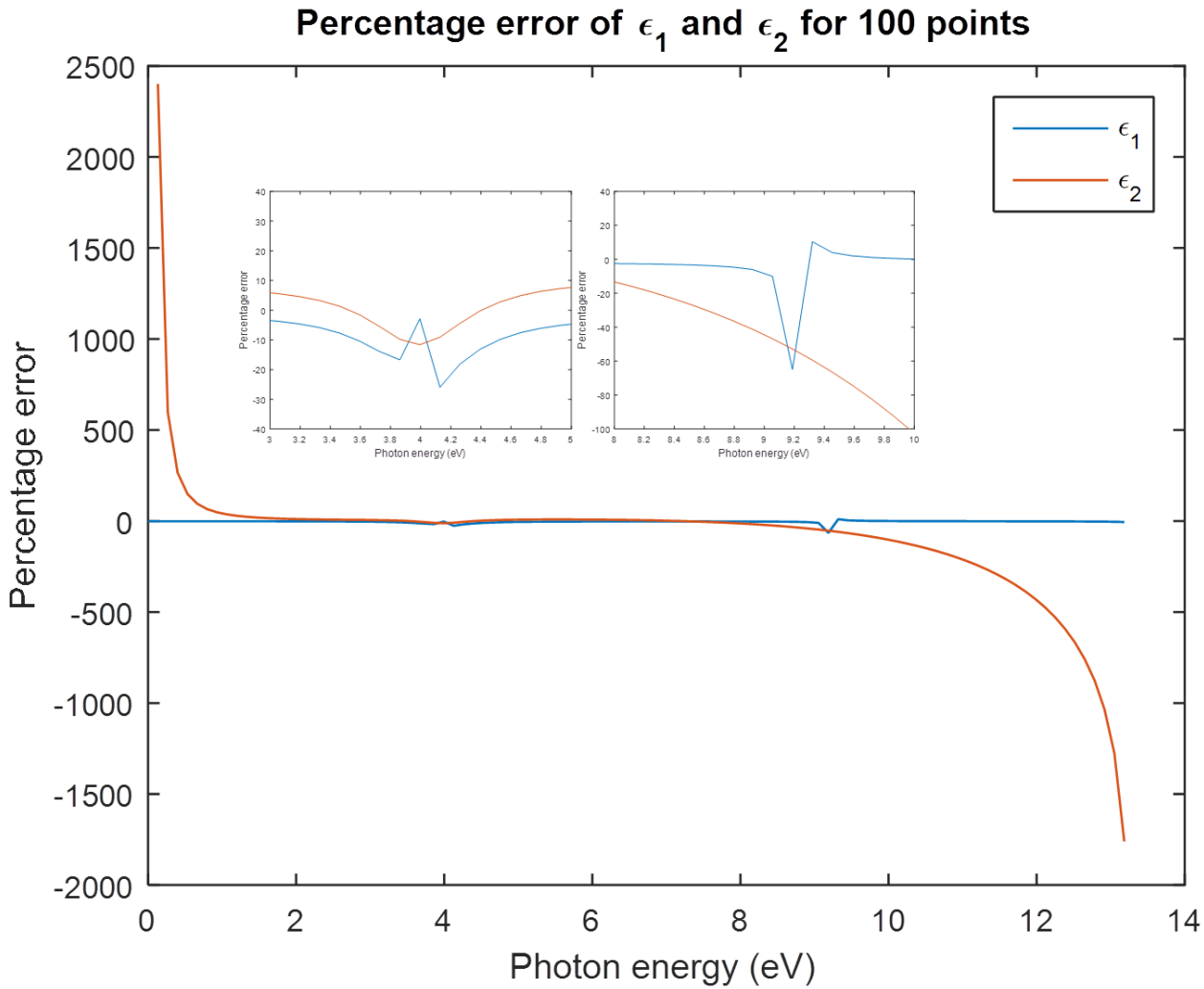

Fig. 3.7. Percentage error between transformed and analytical ϵ (Insert: Magnified view of ϵ at the bumps)

A more rigorous analysis of the transformed ϵ can be made by looking at the percentage error between the analytical and transformed ϵ (Fig. 3.7).

From Fig. 3.5 and Fig. 3.6 it is evident that the Kramers-Kronig transformations stay reasonably faithful to the analytical values. However, extreme care must be taken to account for certain artifacts that may be introduced, such as the "peak" in ϵ_2 near 0.1 eV. The peak occurs at the edge due to the absence of values to the left, and is unique to the way the transformation is handled. In actual experimental data, the data range usually starts just before the bandgap, and such artifacts in ϵ_2 may be mistaken for a false Drude response that may be misinterpreted as Excitonic effects. A quick and dirty way to avoid such problems is simply to truncate the edges. However, while that removes the obvious "peak", other artifacts such as the reduced spectral weights of the real peaks are less easily remedied.

From Fig. 3.7, we see dramatic percentage errors for ϵ_2 at the edges of the data. However, a closer examination and comparison with Fig. 3.6 reveals that these are due to the near-zero ϵ_2 values at these energies. A similar effect can be observed in Fig. 3.7 in the little spikes around 4 and 9.2 eV for ϵ_1.

A natural question that arises from the above is whether these errors can be reduced by "improving" the Riemann sum's approximation to the integral. First, the data points should be as dense as possible such that $d\omega \to 0$. Second, the energy range should be as large as possible to approach $\int_0^\infty$. The 2 hypotheses are tested in the following sections, Section 3.3.4 and Section 3.3.5 respectively.

3.3.4 Varying dω

The same approach and analysis as Section 3.3.2 was used to compare the Kramers-Kronig transformation for 50 and 1000 data points. The results are shown in Fig. 3.8.

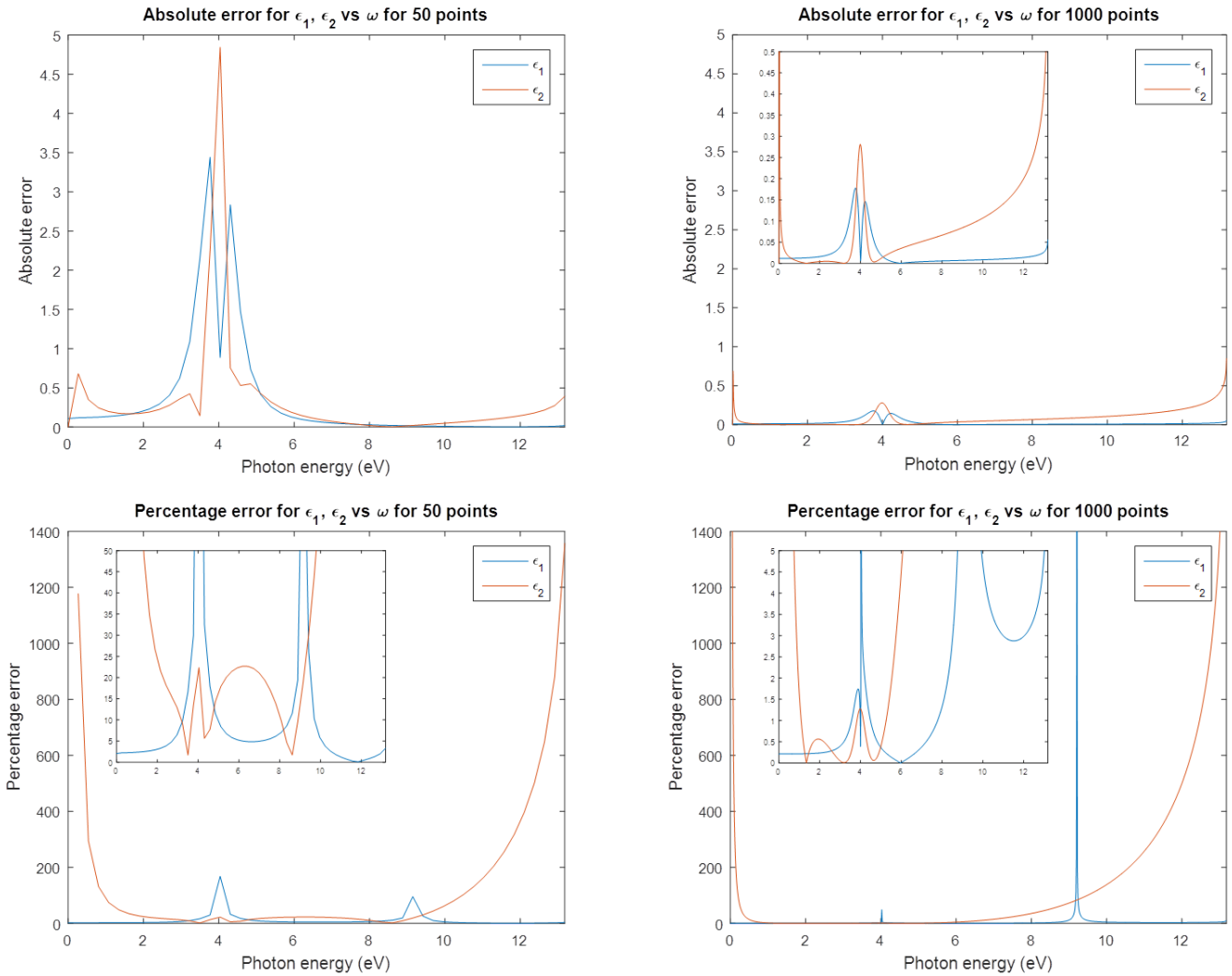

Fig. 3.8. Errors between transformed and analytical ϵ for 50 and 1000 data points (Inserts: Magnified views)

From Fig. 3.8, it is clear that increasing data point density leads to reduced absolute errors. A cursory look at the percentage graphs gives the following:

- the percentage error of ϵ_1 has 2 sharp peaks at 4 and 9 eV, and is slowly increasing around 12 eV
- the percentage error of ϵ_2 is high at 0 and 12 eV, and generally small in between

Generally, from the absolute error graphs, we expect a decrease in error as the number of points is increased. Consider 4eV (the location of our Lorentzian peak in Fig. 3.3, which is usually the region of interest): we can see a sharp decrease in percentage error of ϵ_2 from 20% to 1%, which is expected. However, the percentage error of ϵ_1 at 4eV behaves differently. The explanation for these "abnormal percentage error peaks" are readily available from Fig. 3.5 and Fig. 3.6: ϵ values are near zero at these energy values.

The inserts in Fig. 3.8 highlight a possible error that may be introduced in the transformation process: the percentage error of ϵ_2 is expected to blow up at higher energies as its analytical value approaches zero, but the form of the percentage error for our 1000 points data set is different from that of 50 points from 4 eV onwards. The reason for this is revealed in the insert in Fig. 3.6: the analytical form of ϵ_2 approaches zero at high energies, while the transformed ϵ_2 crosses zero at some point and nose-dives into negative values. This greatly affects the shape of the transformed ϵ_2 graph from 4 eV onwards. No simple solution for this exists, and is an important effect to consider near the high energy edge of the data set when performing the transformation.

3.3.5 Varying energy range

The same approach and analysis as Section 3.3.2 was used to compare the Kramers-Kronig transformation for energy ranges of 1×10^{16} rad/s ($\approx$ 6.5 eV) and 3×10^{16} rad/s ($\approx$ 20 eV). The results are shown in Fig. 3.9.

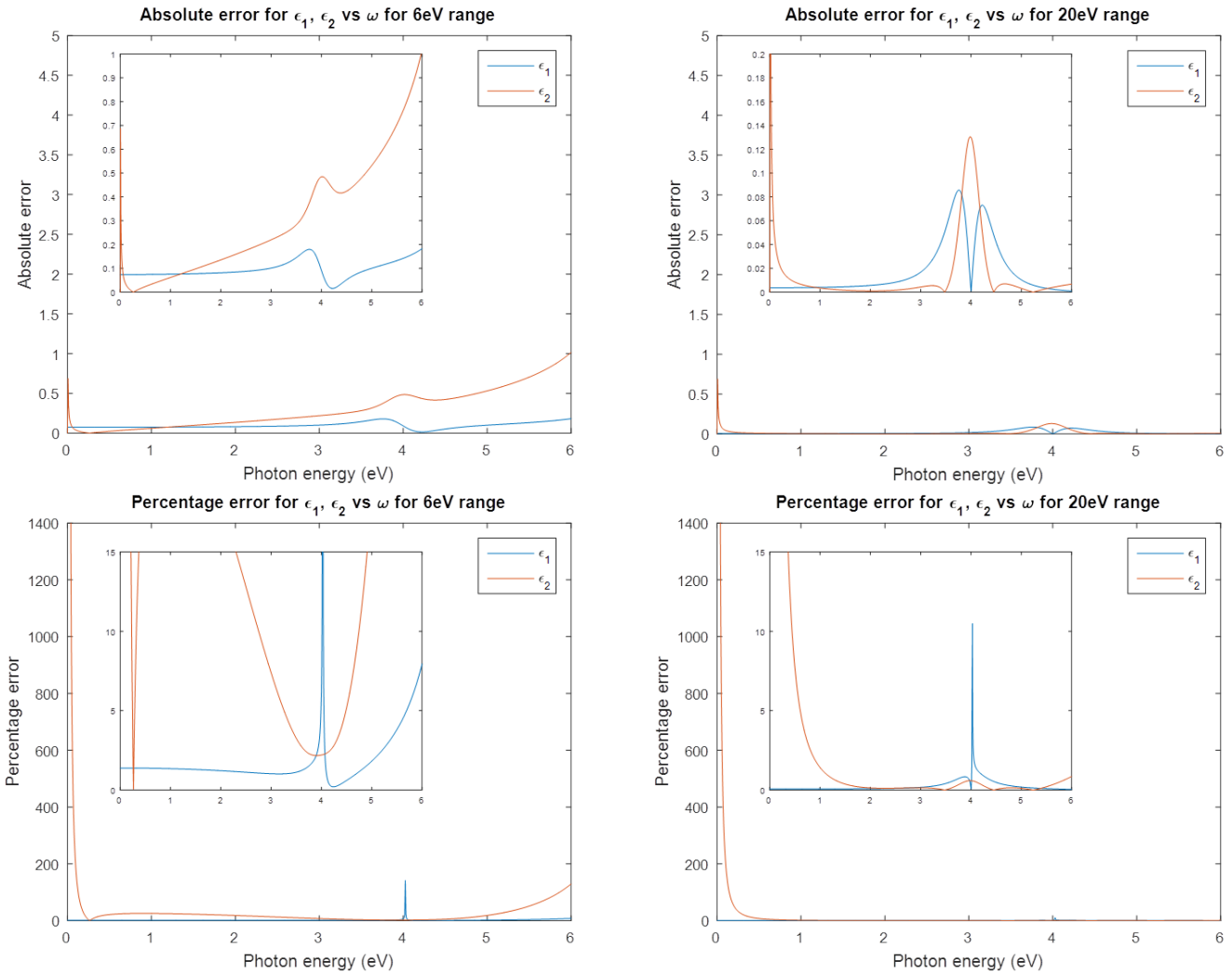

Fig. 3.9. Errors between transformed and analytical ϵ for 6.5 eV and 20 eV (Inserts: Magnified views)

Note that both graphs have been truncated to 6 eV for easier comparison. A set of untruncated percentage error graphs is given in Fig. 3.10. There is a 9 eV peak

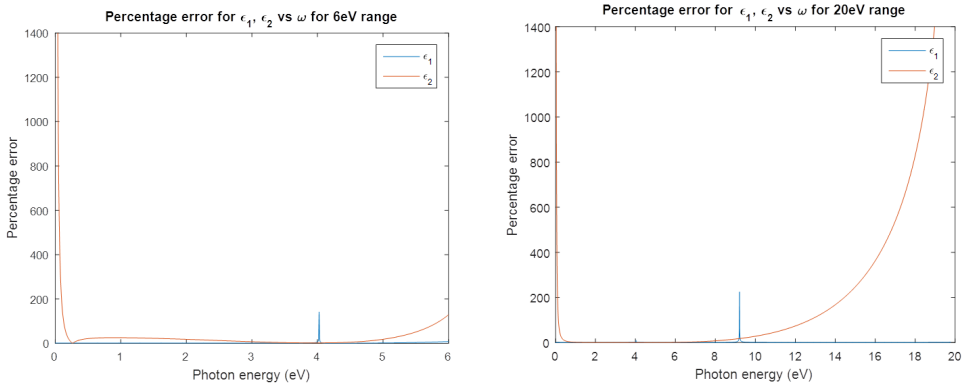

Fig. 3.10. Percentage error of ϵ for different ranges

in the percentage error ϵ_1 for 20 eV range due to the zero-crossing, as expected. Truncating the 20eV graph will also cut out the large percentage errors at large energy values (an effect already observed in Section 3.3.4). Other than that, the truncation leads to no further loss of information as we are more concerned with the region around 4 eV.

As before, we notice a decrease in absolute errors in Fig. 3.9 as we improve the transformation conditions (by increasing the range in this case). The same analysis in Section 3.3.4 can be applied, and we can confirm the following:

- the percentage error of ϵ_1 spikes at 4 eV, but this is due to the near-zero value of ϵ_1
- the percentage error of ϵ_2 is large at the edges of the energy range, and a small peak at 4 eV

The ϵ_2 peak at 4 eV for the 6 eV range data set is washed out by the large percentage errors at 0 and 6 eV. This highlights the importance of using a wide energy range around the region of interest when using the Kramers-Kronig transformation. Comparing Fig. 3.10 and Fig. 3.9, we notice that percentage error of ϵ_2 is greatly reduced at 4 eV when a 20 eV range is used as compared to when a 6.5 eV range was used.

3.3.6 Bulk $SrTiO_3$

Armed with the insights gained from our toy model, we can extend our analysis to the data from our bulk STO sample. ϵ_1 and ϵ_2 values were obtained from Fig. 3.1, the Kramers-Kronig transformation applied, and the same error analysis as above is performed. We can also reverse-calculate ρ from the transformed ϵ using (3.4) [1] and compare it with the experimental ρ as obtained from Ψ and Δ. The transformed ϵ is compared in Fig. 3.11, and the transformed ρ in Fig. 3.12.

$$\rho = \frac{sin^2\theta_0 - cos\theta_0[\epsilon - sin^2\theta_0]^{1/2}}{sin^2\theta_0 + cos\theta_0[\epsilon - sin^2\theta_0]^{1/2}} \tag{3.4}$$

[1] See Appendix B for derivation

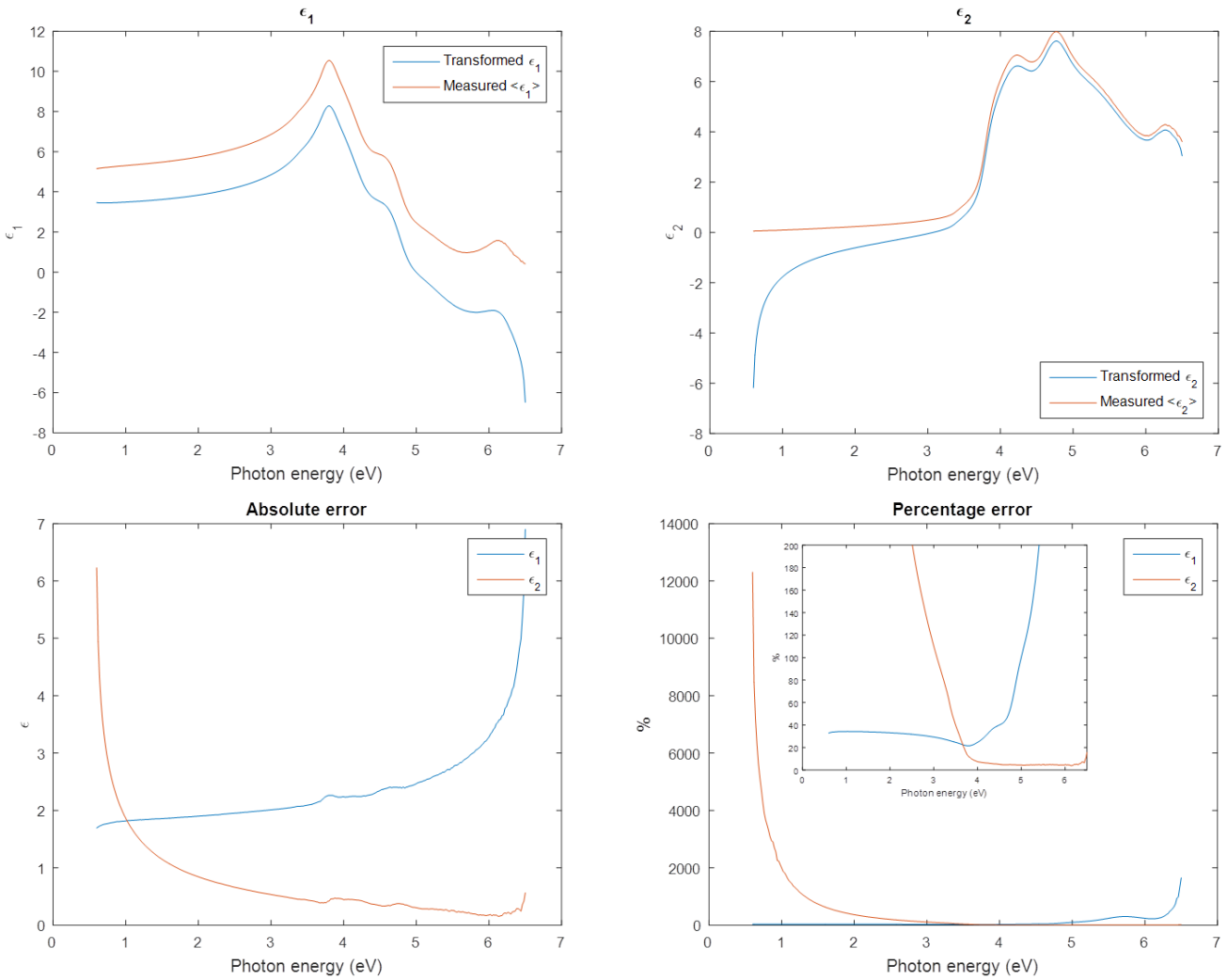

Fig. 3.11. Comparison between transformed and experimental ϵ (Insert: Magnified view)

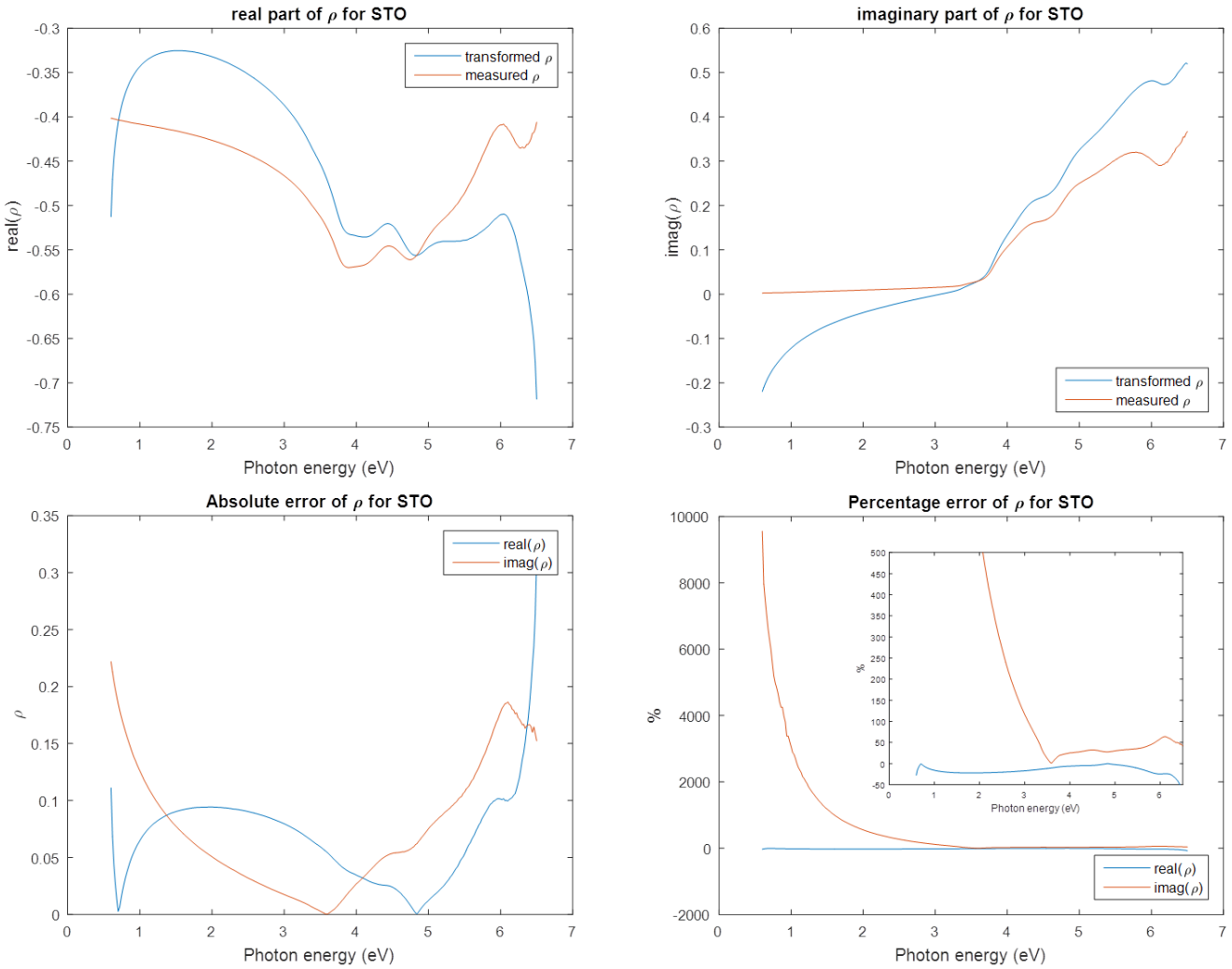

Fig. 3.12. Comparison between transformed and experimental ρ (Insert: Magnified view)

Given that our data point density is 1 point per 0.02 eV and a spectral range of 0.6 to 6.5 eV was used, it is perhaps not too surprising that such large errors still exist. However, the data set represents the typical measurement parameters used, and this highlights the non-triviality of the errors introduced by the Kramers-Kronig transformation when applying it to experimental data.

3.3.7 Final remarks on the Kramers-Kronig transformation

The analysis of the Kramers-Kronig transformation performed in this section reveals that the error introduced during the transformation is non-trivial.

- Parameters like data point density ($d\omega$) and the energy range will affect the quality of the transformation.
- Transformed values are unreliable near the edges of the energy range.
- Care must be taken when quoting percentage error values near zero-crossings. This is especially troublesome when performing error analysis for ϵ_1 since the crossing will occur at the energy value of the Lorentzian peak.
- The exact algorithm used to perform the transform must be considered. In our case, the simple algorithm used introduced numerous artifacts, with the small peak in ϵ_2 at the minimum energy especially severe as it could be mistaken for a Drude response.

The error that will be introduced if we apply the transformation on our substrate data was shown in Section 3.3.6. The Kramers-Kronig constraint can be used when extracting the optical properties of a thin film on substrate in ellipsometry, but as shown here, a direct application of the transformation conditions will introduce large errors. Modified forms of the constraint exist [29, 30] that may be able to circumvent these large errors and will be examined in future work.

One key takeaway from this small exercise is that any published result that extracted a material's optical properties from reflectivity measurements should be

treated with caution. The lack of phase information in reflectivity measurements leads to the prevalence of the Kramers-Kronig transformation in their analysis to extract the material's dielectric functions [13, 14, 15]. Of course, technical limitations in laboratory conditions mean that extrapolation is often required [31], or other approximations and workarounds [22, 32]. However, papers have been published that highlight erroneous analysis resulting from such methods [33], supporting our point that the Kramers-Kronig relations are not to be used lightly even with seemingly appropriate extrapolations, due to the non-triviality of the errors introduced.

For the purpose of this report, however, given that all our MoS_2 on STO data shares similar parameters as our STO data, any method that involves the manual application of the Kramers-Kronig constraint is thus judged to be a poor way to proceed. Method 1 is thus abandoned in favour of method 2. It should be noted that the Kramers-Kronig relation exists intrinsically in the Lorentz model used in method 2, but these are naturally obeyed by the ϵ equations of the model. The additional step of explicitly transforming one of the ϵ values that is required in method 1 is no longer necessary, and thus no such errors will be introduced.

3.4 Insufficiency of 3 layer optical model

Using Matlab, it is possible to create a complex dielectric function model with 3 Lorentzians ((1.27) and (1.28), see Appendix F for the Matlab code). Armed with the substrate data obtained from Section 3.1 and other experimental parameters such as incident angle, we can go one step further and calculate the ρ of this 3-Lorentzian-thin-film on our STO substrate. By comparing this calculated ρ with our experimental ρ of MoS_2 on STO, we can keep adjusting the parameters for our 3-Lorentzian-material until we get a good fit, and thus obtain a fitted solution for ϵ for our MoS_2 thin film.

The thickness of the film is first assumed to be 15.2 angstroms from literature values [20], and may be readjusted during the fitting process to obtain a better fit.

3.4.1 Test fitting of substrate data

To test the validity of the fitting subroutine, an attempt was first made to fit the STO substrate data. The same code as Appendix F is used except that the lorentz model is used to produce N_2 instead of N_1, and N_1 is set to 1. This effectively reduces the expression for ρ into the case for a air-substrate model. The parameter d is left as it is as it no longer affects anything.

The Ψ/Δ plots shown in Fig. 2.1 were converted into ρ using (3.5). The real and imaginary parts can then be plotted separately (Section 3.4.1).

$$\rho = tan(\Psi) \times exp(i\Delta) \tag{3.5}$$

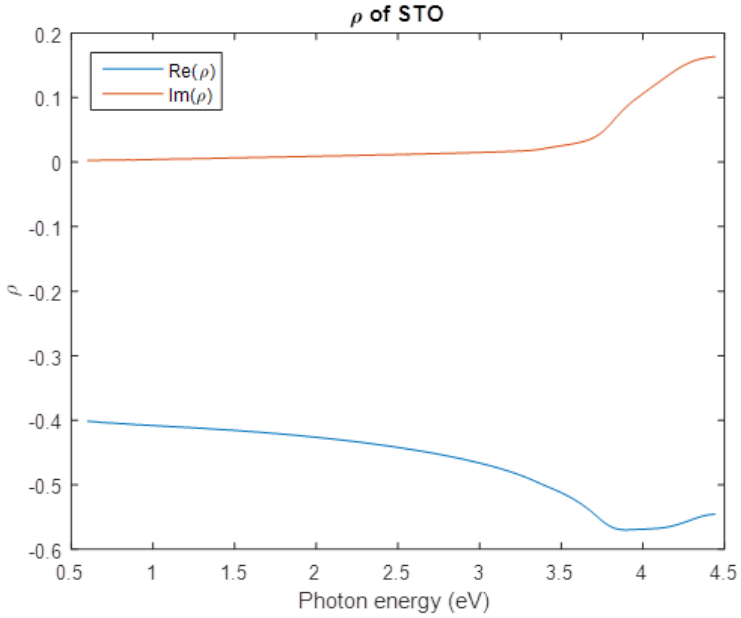

Fig. 3.13. Real and imaginary parts of ρ for STO

Using (3.6) [2] and (3.7) as derived from the Lorentz model, and our expression for ρ, we can attempt to perform the fitting. Using literature values of $E_{0,j}$ [34] and guessing the other parameters, we obtain the fit as shown in Fig. 3.14

[2] the replacement of the constant 1 with ϵ_∞ is simply a convenient accounting of higher order Lorentzians that are not included in our 3-Lorentzian model.

$$\epsilon_1 = \epsilon_\infty + \sum_{j=1}^{3} \frac{A_j(E_{0,j}^2 - E^2)}{(E_{0,j}^2 - E^2)^2 - \Gamma_j^2 E^2} \tag{3.6}$$

$$\epsilon_2 = \sum_{j=1}^{3} \frac{A_j \Gamma_j E}{(E_{0,j}^2 - E^2)^2 - \Gamma_j^2 E^2} \tag{3.7}$$

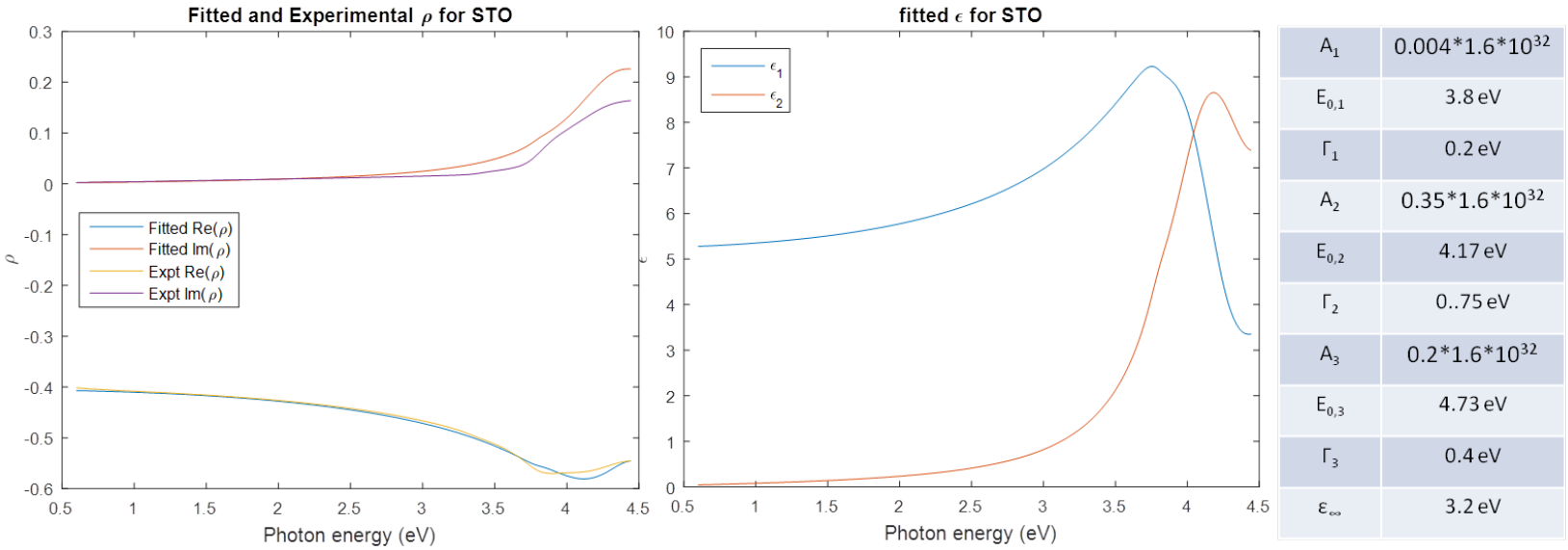

A_1	$0.004*1.6*10^{32}$
$E_{0,1}$	3.8 eV
Γ_1	0.2 eV
A_2	$0.35*1.6*10^{32}$
$E_{0,2}$	4.17 eV
Γ_2	0..75 eV
A_3	$0.2*1.6*10^{32}$
$E_{0,3}$	4.73 eV
Γ_3	0.4 eV
ε_∞	3.2 eV

Fig. 3.14. Fitting of ϵ for STO

The fitted ϵ can be compared to the pseudo dielectric function in Fig. 3.1. It is clear that the fit is not perfect, but the general shape is satisfied. A better fit may be done using commercial programs, but this example is sufficient to demonstrate that our Matlab code for a 3 optical layer (reduced to 2 layer via appropriate substitutions), 3-Lorentzian model is not erroneous.

3.4.2 Unsuccessful fitting of ϵ of MoS_2

As verified earlier, upon removal of the applied assumptions and substitutions in Section 3.4.1, the Matlab code should be able to revert to a working 3-optical-layer, 3-Lorentzian model that we can apply to our MoS_2 on STO data. As before, the Ψ/Δ plots shown in Fig. 2.2 were converted into ρ using (3.5). The real and imaginary parts can then be plotted separately (Fig. 3.15).

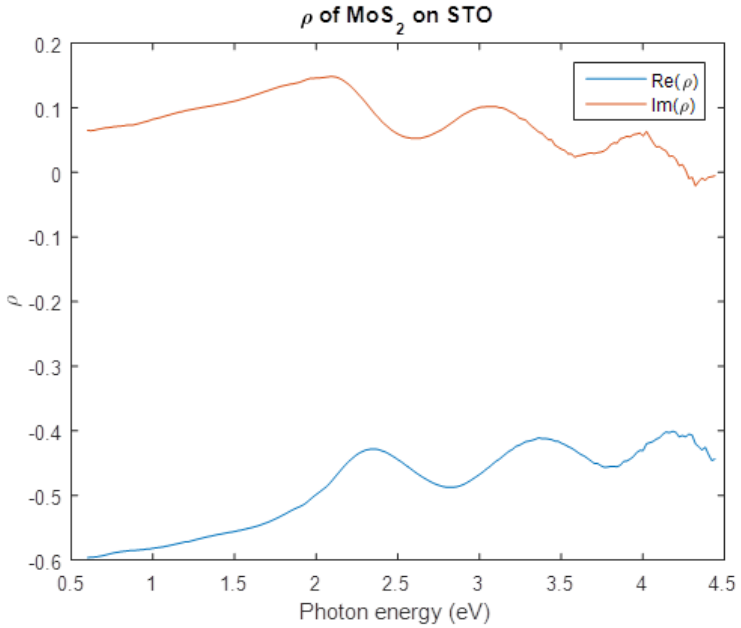

Fig. 3.15. Real and imaginary parts of ρ for MoS_2 on STO

Numerous attempts were made to obtain the complex dielectric function of MoS_2, but none were successful in reproducing the experimental ρ vs photon energy curves (See Appendix G). Possible reasons for this include [12]:

- measured (Ψ,Δ) spectra are inaccurate
- dielectric functions used in data analysis are inappropriate

- the optical model used in data analysis is inappropriate
- the sample has a depolarization effect

Amongst the reasons given, the dielectric function and the optical model are the most suspect. The Lorentz model was chosen for this project due to its robustness, and other models such as the Drude model, Cauchy model etc are derived from the Lorentz model [12]. As such, the cause for the unsuccessful fitting is likely due to a poor choice of the optical model. A simple air-film-substrate model was used, which does not account for interface effects. It has been revealed that interface effects play a large role in polar $LaAlO_3$ on non-polar $SrTiO_3$ structures [35], which suggests that interface effects may not be negligible in our MoS_2 on STO sample. More research is needed to confirm this, and to develop and test a 4 layer optical model that takes interface effects into consideration.

Chapter 4

Conclusion

Given a set of spectroscopic ellipsometry data, one can immediately calculate its pseudo dielectric function without using the Kramers-Kronig transformation or any modeling. However, this $< \epsilon >$ assumes a bulk, perfectly smooth material. When such conditions are satisfied, the pseudo dielectric function is a good approximation to its true dielectric function (Section 1.3.2). While this is valuable information by itself, a dielectric function model is often used to extract more physical insights out of it. The Lorentz model can be used (Section 1.3.3), but it is common to consider certain assumptions to obtain simpler models such as the Sellmeier model [36], Tauc-Lorentz model [37], or hybrid models to better explain certain phenomena [16]. This decomposition of the dielectric function is often done by fitting [12], and the results allow us to identify the oscillator types (eg. excitonic effects, phononic effects, etc [38]).

However, when the sample is not a bulk, perfectly smooth material, an appropriate optical model must be used to properly analyze the ellipsometry data (Section 1.3.2). A judicious choice of model is of paramount importance as shown in this report (Section 3.4). A poor choice of the optical model will not just lead to slightly inaccurate results; in the case of MoS_2 on STO, interface effects play such a large role that a 3 layer optical model fails completely (Section 3.4.2).

Once a good optical model has been chosen, we can once again use a dielectric

function model to obtain a calculated ρ, which can be fitted to the experimental ρ (Section 3.4.1). However, this requires either some prior knowledge of the material, or excellent intuition and luck, as the fitting parameters (A_j, $E_{0,j}$, Γ_j, ϵ_∞ if done manually, tolerance levels and number of oscillators and initial guesses if done by a fitting program that minimizes Chi-square) will greatly affect the results. An alternative method is to solve an "inverse ellipsometry problem": to impose certain constraints (Kramers-Kronig relations [39], or multiple experimental data sets [40]) to solve ϵ_1 and ϵ_2 numerically from the experimental ρ values. Using multiple data sets is difficult as the tangent(Ψ) in the expression for ρ amplifies any experimental errors, often leading to unphysical solutions for ϵ. Using the Kramers-Kronig relations circumvents this problem since only a single data set is used, but the limited spectral range and non-infinitesimal data point density will introduce errors that will in turn affect the calculated ρ (Section 3.3). How this affects the final results is dependent on the exact numerical solution algorithm used, but the errors are expected to be highly non-trivial. Indeed, the constraint is often used in analyzing reflectivity spectra in an attempt to regain the lost phase information, and erroneous results have been reported [33].

We thus see that spectroscopic ellipsometry is highly sensitive to the way the data is treated. While this makes it a difficult technique to use, it is also what makes it so powerful as this sensitivity can unambiguously reveal the presence of surface roughness, interface effects, etc. Indeed, spectroscopic ellipsometry has been used to investigate interface effects to great success [35], and we have also shown in this report that interface effects between MoS_2 bilayer and bulk STO are non-negligible.

Chapter 5

Future Work

Work is ongoing to build a 4 layer optical model using Mathematica and Matlab to better investigate the interface effects between bilayer MoS_2 and STO. However, a general treatment of such a model means that 2 independent sets of dielectric functions (one for the film, one for the interface) must be fitted, which is impossible given just one set of experimental data. One possible approach is to collect multiple data sets at different incident angles [35]. Another possible approach is to perform spectroscopic ellipsometry on a similar sample but with a substrate that does not induce interface effects and then compare the data, but again the analysis will be non-trivial.

More research is also required to study the inverse ellipsometry problem, as modified forms of the Kramers-Kronig transform do exist [22, 32, 29, 30] that are expected to introduce smaller errors. The inverse ellipsometry problem may also be solved by using multiple sets of spectroscopic ellipsometry data instead of the Kramers-Kronig constraint. However, a quick test of this [1] showed that the $tan(\Psi)$ in (1.1) introduces extremely large variations in ρ values that makes a numerical solution difficult and unreliable. This method has been shown to be successful under certain conditions [40] but a general treatment is difficult, and much more study is required.

[1] a similar code to Appendix F was used to solve for ϵ values for data taken at 2 different incident angles using the numerical solver function *vpasolve*, but only nonsensical results were obtained.

A more in-depth study into the field of statistics is also required to properly quantify fitting errors.

Bibliography

[1] J. Powell, "The quantum limit to moore's law," *Proceedings of the IEEE*, vol. 96, no. 8, pp. 1247–1248, Aug 2008.

[2] L. B. Kish, "End of moore's law: thermal (noise) death of integration in micro and nano electronics," *Physics Letters A*, vol. 305, no. 34, pp. 144 – 149, 2002. [Online]. Available: http://www.sciencedirect.com/science/article/pii/S0375960102013658

[3] F. Schwierz, "Graphene transistors," *Nat Nano*, vol. 5, no. 7, pp. 487–496, Jul 2010. [Online]. Available: http://dx.doi.org/10.1038/nnano.2010.89

[4] X. Chen, L. Wang, W. Li, Y. Wang, Z. Wu, M. Zhang, Y. Han, Y. He, and N. Wang, "Electronelectron interactions in monolayer graphene quantum capacitors," *Nano Research*, 2013.

[5] G. Fiori and G. Iannaccone, "On the possibility of tunable-gap bilayer graphene fet," *Electron Device Letters, IEEE*, vol. 30, no. 3, pp. 261–264, March 2009.

[6] F. Schwierz, "Graphene transistors: Status, prospects, and problems," *Proceedings of the IEEE*, vol. 101, no. 7, pp. 1567–1584, July 2013.

[7] Q. H. Wang, K. Kalantar-Zadeh, A. Kis, J. N. Coleman, and M. S. Strano, "Electronics and optoelectronics of two-dimensional transition metal dichalcogenides," *NATURE NANOTECHNOLOGY*, 2012.

[8] W.-H. Kim and J. Y. Son, "Single-layer mos2 field effect transistor with epitaxially grown srtio3 gate dielectric on nb-doped srtio3 substrate,"

Bull. Korean Chem. Soc, vol. 34, 2013. [Online]. Available: http://dx.doi.org/10.5012/bkcs.2013.34.9.2563

[9] M. Ohring, *Materials Science of Thin Films*. Elsevier Science, 2001. [Online]. Available: https://books.google.com.sg/books?id=m3fai5hbc94C

[10] H. Moser, C. Diao, B. Casse, E. Chew, M. Cholewa, S. Ding, J. Kong, and Z. Li, "Singapore synchrotron light source - helios2 and beyond," *Proceedings of EPAC*, 2004.

[11] R. L. Johnson, J. Barth, M. Cardona, D. Fuchs, and A. M. Bradshaw, "Spectroscopic ellipsometry with synchrotron radiation," *Review of Scientific Instruments*, 1988.

[12] H. Fujiwara, *Spectroscopic Ellipsometry: Principles and Applications*. John Wiley and Sons Ltd, 2007.

[13] A. R. Beal and H. P. Hughes, "Kramers-kronig analysis of the reflectivity spectra of 2h-mos 2 , 2h-mose 2 and 2h-mote 2," *Journal of Physics C: Solid State Physics*, vol. 12, no. 5, p. 881, 1979. [Online]. Available: http://stacks.iop.org/0022-3719/12/i=5/a=017

[14] W. C. Walker and J. Osantowski, "Ultraviolet optical properties of diamond," *Phys. Rev.*, vol. 134, pp. A153–A157, Apr 1964. [Online]. Available: http://link.aps.org/doi/10.1103/PhysRev.134.A153

[15] P. Grosse and V. Offermann, "Analysis of reflectance data using the kramers-kronig relations," *Applied Physics A*, vol. 52, no. 2, pp. 138–144, 1991.

[16] B. Mukherjee, F. Tseng, D. Gunlycke, K. K. Amara, G. Eda, and E. Simsek, "Complex electrical permittivity of the monolayer molybdenum disulfide (mos 2) in near uv and visible," *Optical Materials Express*, vol. 5, no. 2, pp. 447–455, 2015.

[17] D. J. Griffiths, *Introduction to Electrodynamics*. Pearson, 2013.

[18] S. Russev and D. Georgieva, "Analytical solution of another ellipsometric inverse problem," *Journal of Modern Optics*, vol. 38, no. 7, pp. 1217–1222, 1991. [Online]. Available: http://dx.doi.org/10.1080/09500349114551381

[19] M. Wakagi, H. Fujiwara, and R. Collins, "Real time spectroscopic ellipsometry for characterization of the crystallization of amorphous silicon by thermal annealing," *Thin Solid Films*, vol. 313314, pp. 464 – 468, 1998. [Online]. Available: http://www.sciencedirect.com/science/article/pii/S0040609097008651

[20] Y. L. Huang, Y. Chen, W. Zhang, S. Y. Quek, C.-H. Chen, L.-J. Li, W.-T. Hsu, W.-H. Chang, Y. J. Zheng, W. Chen, and A. T. S. Wee, "Bandgap tunability at single-layer molybdenum disulphide grain boundaries," *Nat Commun*, vol. 6, Feb 2015, article. [Online]. Available: http://dx.doi.org/10.1038/ncomms7298

[21] Y. Li, Z. Qi, M. Liu, Y. Wang, X. Cheng, G. Zhang, and L. Sheng, "Photoluminescence of monolayer mos2 on laalo3 and srtio3 substrates," *Nanoscale*, vol. 6, pp. 15 248–15 254, 2014. [Online]. Available: http://dx.doi.org/10.1039/C4NR04602A

[22] D. Roessler, "Kramers-kronig analysis of reflection data," *British Journal of Applied Physics*, vol. 16, no. 8, p. 1119, 1965.

[23] H. Balian and N. W. Eddy, "Figure-of-merit (fom), an improved criterion over the normalized chi-squared test for assessing goodness-of-fit of gamma-ray spectral peaks," *Nuclear Instruments and Methods*, vol. 145, no. 2, pp. 389 – 395, 1977. [Online]. Available: http://www.sciencedirect.com/science/article/pii/0029554X77904372

[24] Y. Liu, J. Hsieh, and S. Tung, "Extraction of optical constants of zinc oxide thin films by ellipsometry with various models," *Thin Solid*

Films, vol. 510, no. 12, pp. 32 – 38, 2006. [Online]. Available: http://www.sciencedirect.com/science/article/pii/S0040609006001775

[25] J.-P. Xu, R.-J. Zhang, Z.-H. Chen, Z.-Y. Wang, F. Zhang, X. Yu, A.-Q. Jiang, Y.-X. Zheng, S.-Y. Wang, and L.-Y. Chen, "Optical properties of epitaxial bifeo3 thin film grown on srruo3-buffered srtio3 substrate," *Nanoscale Research Letters*, vol. 9, no. 1, pp. 1–6, 2014. [Online]. Available: http://dx.doi.org/10.1186/1556-276X-9-188

[26] Y. Kyung Lim and H. J Lee, "Causality, kramers-kronig relations, and landau damping," *The Open Plasma Physics Journal*, vol. 5, no. 1, 2012.

[27] K. R. Waters, J. Mobley, and J. G. Miller, "Causality-imposed (kramers-kronig) relationships between attenuation and dispersion," *IEEE Transactions on Ultrasonics, Ferroelectrics, and Frequency Control*, vol. 52, no. 5, pp. 822–823, May 2005.

[28] D. Natelson. What are the kramers-kronig relations, physically? [Online]. Available: http://nanoscale.blogspot.sg/2014/05/what-are-kramers-kronig-relations.html

[29] R. Ahrenkiel, "Modified kramers–kronig analysis of optical spectra," *JOSA*, vol. 61, no. 12, pp. 1651–1655, 1971.

[30] J. E. Bertie and Z. Lan, "An accurate modified kramers–kronig transformation from reflectance to phase shift on attenuated total reflection," *The Journal of chemical physics*, vol. 105, no. 19, pp. 8502–8514, 1996.

[31] G. Leveque, "Reflectivity extrapolations in kramers-kronig analysis," *Journal of Physics C: Solid State Physics*, vol. 10, no. 23, p. 4877, 1977.

[32] N. I. Stas'kov and A. V. Shulga, "Solution of the inverse spectroscopic ellipsometry problem for an absorbing substrate with a dielectric layer," *Journal of Applied Spectroscopy*, pp. 1–7, 2016. [Online]. Available: http://dx.doi.org/10.1007/s10812-016-0239-8

[33] H. R. Phillip and E. A. Taft, "Kramers-kronig analysis of reflectance data for diamond," *Phys. Rev.*, vol. 136, pp. A1445–A1448, Nov 1964. [Online]. Available: http://link.aps.org/doi/10.1103/PhysRev.136.A1445

[34] S. Zollner, A. Demkov, R. Liu, P. Fejes, R. Gregory, P. Alluri, J. Curless, Z. Yu, J. Ramdani, R. Droopad *et al.*, "Optical properties of bulk and thin-film srtio3 on si and pt," *Journal of Vacuum Science and Technology B*, vol. 18, no. 4, pp. 2242–2254, 2000.

[35] T. C. Asmara, I. Santoso, and A. Rusydi, "Self-consistent iteration procedure in analyzing reflectivity and spectroscopic ellipsometry data of multilayered materials and their interfaces," *Review of Scientific Instruments*, vol. 85, no. 12, 2014. [Online]. Available: http://scitation.aip.org/content/aip/journal/rsi/85/12/10.1063/1.4897487

[36] C. M. Nelson, M. Spies, L. S. Abdallah, S. Zollner, Y. Xu, and H. Luo, "Dielectric function of laalo3 from 0.8 to 6 ev between 77 and 700 k," *Journal of Vacuum Science & Technology A*, vol. 30, no. 6, p. 061404, 2012.

[37] C. Yim, M. O'Brien, N. McEvoy, S. Winters, I. Mirza, J. G. Lunney, and G. S. Duesberg, "Investigation of the optical properties of mos2 thin films using spectroscopic ellipsometry," *Applied Physics Letters*, vol. 104, no. 10, p. 103114, 2014.

[38] P. K. Gogoi, L. Sponza, D. Schmidt, T. C. Asmara, C. Diao, J. C. W. Lim, S. M. Poh, S.-i. Kimura, P. E. Trevisanutto, V. Olevano, and A. Rusydi, "Anomalous excitons and screenings unveiling strong electronic correlations in $\mathrm{srti}_{1-x}\mathrm{nb}_x\mathrm{o}_3 (0 \leq x \leq 0.005)$," *Phys. Rev. B*, vol. 92, p. 035119, Jul 2015. [Online]. Available: http://link.aps.org/doi/10.1103/PhysRevB.92.035119

[39] A. Kuzmenko, "Kramers–kronig constrained variational analysis of optical spectra," *Review of scientific instruments*, vol. 76, no. 8, p. 083108, 2005.

[40] F. Sagnard, "Determination of complex permittivity and thickness of a single-layer material using reflection ellipsometry at several angles of incidence," *Microwave and Optical Technology Letters*, vol. 35, no. 2, pp. 154–157, 2002.

[41] V. Scarani, *PC4246 Lecture on Quantum Optics*. National University of Singapore.

Appendix A

Definition of optical constants used

This report adopts the Optics convention for the definitions listed below.

Table A2.1 Definitions of the optical constants used in the optics and physics fields

	Optics	Physics	Section
Phase of light	$(\omega t - Kx + \delta)$	$(Kx - \omega t + \delta)$	2.1.1
When the initial phase δ is positive	Wave advances	Wave lags	3.1.1
Complex refractive index	$N \equiv n - \mathrm{i}k$	$N \equiv n + \mathrm{i}k$	2.1.3
Complex dielectric constant	$\varepsilon \equiv \varepsilon_1 - \mathrm{i}\varepsilon_2$	$\varepsilon \equiv \varepsilon_1 + \mathrm{i}\varepsilon_2$	2.2.2
Optical interference	$r_{012} = \dfrac{r_{01} + r_{12}\exp(-\mathrm{i}2\beta)}{1 + r_{01}r_{12}\exp(-\mathrm{i}2\beta)}$	$r_{012} = \dfrac{r_{01} + r_{12}\exp(\mathrm{i}2\beta)}{1 + r_{01}r_{12}\exp(\mathrm{i}2\beta)}$	2.4.1
Right-circular polarization	$\dfrac{1}{\sqrt{2}}\begin{bmatrix}1\\ \mathrm{i}\end{bmatrix}$	$\dfrac{1}{\sqrt{2}}\begin{bmatrix}1\\ -\mathrm{i}\end{bmatrix}$	3.3.1
Left-circular polarization	$\dfrac{1}{\sqrt{2}}\begin{bmatrix}1\\ -\mathrm{i}\end{bmatrix}$	$\dfrac{1}{\sqrt{2}}\begin{bmatrix}1\\ \mathrm{i}\end{bmatrix}$	3.3.1
(ψ, Δ)	$\rho \equiv \tan\psi\exp(\mathrm{i}\Delta)$	$\rho \equiv \tan\psi\exp(-\mathrm{i}\Delta)$	4.1.1
Lorentz model	$\varepsilon = 1 + \dfrac{A}{\omega_0^2 - \omega^2 + \mathrm{i}\Gamma\omega}$	$\varepsilon = 1 + \dfrac{A}{\omega_0^2 - \omega^2 - \mathrm{i}\Gamma\omega}$	5.2.1
Drude model	$\varepsilon = \varepsilon_\infty\left(1 - \dfrac{\omega_p^2}{\omega^2 - \mathrm{i}\omega\Gamma}\right)$	$\varepsilon = \varepsilon_\infty\left(1 - \dfrac{\omega_p^2}{\omega^2 + \mathrm{i}\omega\Gamma}\right)$	5.2.5
Pseudo-dielectric function	$\langle\varepsilon\rangle \equiv \langle\varepsilon_1\rangle - \mathrm{i}\langle\varepsilon_2\rangle$	$\langle\varepsilon\rangle \equiv \langle\varepsilon_1\rangle + \mathrm{i}\langle\varepsilon_2\rangle$	5.4.2
Berreman's equation	$\dfrac{\partial\Psi}{\partial z} = -\mathrm{i}\dfrac{\omega}{c}\Delta_B\Psi$	$\dfrac{\partial\Psi}{\partial z} = \mathrm{i}\dfrac{\omega}{c}\Delta_B\Psi$	6.3.1

Fig. A.1. Adopted from Spectroscopic Ellipsometry: Principles and Applications by H. Fujiwara [12]

Appendix B

ρ for the case of medium/substrate interface (Mathematica code)

For the case of ellipsometry on a bulk material, the expression for ρ is relatively simple, and here we can obtain an expression for ϵ as a function of the experimentally obtained ρ.

(* This is the expression for r_p as obtained from the Fresnel equations *)

$$r_p = (n_t * \text{Cos}[\theta_i] - n_i * \text{Cos}[\theta_t]) / (n_t * \text{Cos}[\theta_i] + n_i * \text{Cos}[\theta_t])$$

$$\frac{-\text{Cos}[\theta_t] n_i + \text{Cos}[\theta_i] n_t}{\text{Cos}[\theta_t] n_i + \text{Cos}[\theta_i] n_t}$$

(* This is the expression for r_s as obtained from the Fresnel equations *)

$$r_s = (n_i * \text{Cos}[\theta_i] - n_t * \text{Cos}[\theta_t]) / (n_i * \text{Cos}[\theta_i] + n_t * \text{Cos}[\theta_t])$$

$$\frac{\text{Cos}[\theta_i] n_i - \text{Cos}[\theta_t] n_t}{\text{Cos}[\theta_i] n_i + \text{Cos}[\theta_t] n_t}$$

(* This is the expression for ρ by definition *)

$$\rho = r_p / r_s$$

$$\frac{(-\text{Cos}[\theta_t] n_i + \text{Cos}[\theta_i] n_t)(\text{Cos}[\theta_i] n_i + \text{Cos}[\theta_t] n_t)}{(\text{Cos}[\theta_t] n_i + \text{Cos}[\theta_i] n_t)(\text{Cos}[\theta_i] n_i - \text{Cos}[\theta_t] n_t)}$$

(* Here, we insert Snell's Law to relate θ_t to θ_i *)

$$\theta_t = \text{ArcSin}[(n_i / n_t) * \text{Sin}[\theta_i]]$$

$$\text{ArcSin}\left[\frac{\text{Sin}[\theta_i] n_i}{n_t}\right]$$

(* Here, we insert the relation between n and ϵ, for both incident and transmission materials *)

$$n_i = (\epsilon_i)^{1/2}$$

$$n_t = (\epsilon_t)^{1/2}$$

$$\sqrt{\epsilon_i}$$

$$\sqrt{\epsilon_t}$$

(* Now, we put everything back into ρ *)

FullSimplify[ρ]

$$\frac{\text{Sin}[\theta_i]^2\sqrt{\epsilon_i}-\text{Cos}[\theta_i]\sqrt{1-\frac{\text{Sin}[\theta_i]^2\epsilon_i}{\epsilon_t}}\sqrt{\epsilon_t}}{\text{Sin}[\theta_i]^2\sqrt{\epsilon_i}+\text{Cos}[\theta_i]\sqrt{1-\frac{\text{Sin}[\theta_i]^2\epsilon_i}{\epsilon_t}}\sqrt{\epsilon_t}}$$

(* Now we reexpress ϵ_t in terms of the other terms *)

ClearAll

Quit[]

ClearAll

Solve $\left[\rho==\frac{\text{Sin}[\theta_i]^2\sqrt{\epsilon_i}-\text{Cos}[\theta_i]\sqrt{1-\frac{\text{Sin}[\theta_i]^2\epsilon_i}{\epsilon_t}}\sqrt{\epsilon_t}}{\text{Sin}[\theta_i]^2\sqrt{\epsilon_i}+\text{Cos}[\theta_i]\sqrt{1-\frac{\text{Sin}[\theta_i]^2\epsilon_i}{\epsilon_t}}\sqrt{\epsilon_t}},\epsilon_t\right]$

$$\left\{\left\{\epsilon_t\to\frac{\left(1+\rho^2+2\rho\text{Cos}[2\theta_i]\right)\epsilon_i\text{Tan}[\theta_i]^2}{(1+\rho)^2}\right\}\right\}$$

Appendix C

ρ for the case of medium/thinfilm/substrate (Mathematica code)

Interference effects due to the thin-film can be taken into account to obtain an expression for ρ. The expression is then exported into Matlab directly.

(* rptot and rstot are based on medium/thinfilm/ substrate model, while rp01, rp12, rs01, rs12 are just from Fresnel eqns *)

ClearAll

ClearAll

$\rho = \text{rptot/rstot}$

$\frac{\text{rptot}}{\text{rstot}}$

$\text{rptot} = (\text{rp01} + \text{rp12} * \text{Exp}[-2I\beta])/(1 + \text{rp01} * \text{rp12} * \text{Exp}[-2I\beta])$

$\frac{\text{rp01}+e^{-2i\beta}\text{rp12}}{1+e^{-2i\beta}\text{rp01rp12}}$

$\text{rstot} = (\text{rs01} + \text{rs12} * \text{Exp}[-2I\beta])/(1 + \text{rs01} * \text{rs12} * \text{Exp}[-2I\beta])$

$\frac{\text{rs01}+e^{-2i\beta}\text{rs12}}{1+e^{-2i\beta}\text{rs01rs12}}$

$\text{rp01} = (\text{n1} * \text{Cos}[\theta 0] - \text{n0} * \text{Cos}[\theta 1])/(\text{n1} * \text{Cos}[\theta 0] + \text{n0} * \text{Cos}[\theta 1])$

$\frac{\text{n1Cos}[\theta 0]-\text{n0Cos}[\theta 1]}{\text{n1Cos}[\theta 0]+\text{n0Cos}[\theta 1]}$

$\text{rp12} = (\text{n2} * \text{Cos}[\theta 1] - \text{n1} * \text{Cos}[\theta 2])/(\text{n2} * \text{Cos}[\theta 1] + \text{n1} * \text{Cos}[\theta 2])$

$\frac{\text{n2Cos}[\theta 1]-\text{n1Cos}[\theta 2]}{\text{n2Cos}[\theta 1]+\text{n1Cos}[\theta 2]}$

$\text{rs01} = (\text{n0} * \text{Cos}[\theta 0] - \text{n1} * \text{Cos}[\theta 1])/(\text{n0} * \text{Cos}[\theta 0] + \text{n1} * \text{Cos}[\theta 1])$

$\frac{\text{n0Cos}[\theta 0]-\text{n1Cos}[\theta 1]}{\text{n0Cos}[\theta 0]+\text{n1Cos}[\theta 1]}$

$\text{rs12} = (\text{n1} * \text{Cos}[\theta 1] - \text{n2} * \text{Cos}[\theta 2])/(\text{n1} * \text{Cos}[\theta 1] + \text{n2} * \text{Cos}[\theta 2])$

$\frac{\text{n1Cos}[\theta 1]-\text{n2Cos}[\theta 2]}{\text{n1Cos}[\theta 1]+\text{n2Cos}[\theta 2]}$

(* relationship between θ1, 2, 0 are based on Snell' s law *)

θ1 = ArcCos[√(1 − ((1/n1) ∗ Sin[θ0])^2)]

$$\text{ArcCos}\left[\sqrt{1-\frac{\text{Sin}[\theta 0]^2}{\text{n1}^2}}\right]$$

θ2 = ArcCos[√(1 − ((n1/n2) ∗ Sin[θ1])^2)]

$$\text{ArcCos}\left[\sqrt{1-\frac{\text{Sin}[\theta 0]^2}{\text{n2}^2}}\right]$$

FullSimplify[β = 2πdn1Cos[θ1]/λ]

$$\frac{2d\text{n1}\pi\sqrt{1-\frac{\text{Sin}[\theta 0]^2}{\text{n1}^2}}}{\lambda}$$

(* To make things simpler for later calculations *)

Assumptions → d ∈ Reals

Assumptions → λ ∈ Reals

Assumptions → 0 < θ0 < π/2

$\text{Assumptions} \to d \in \text{Reals}$

$\text{Assumptions} \to \lambda \in \text{Reals}$

$\text{Assumptions} \to 0 < \theta 0 < \frac{\pi}{2}$

(* Now to obtain the final expression for ρ *)

FullSimplify[ρ]

$$\frac{\left(\frac{\text{n1}\cos[\theta 0]-\text{n0}\sqrt{1-\frac{\sin[\theta 0]^2}{\text{n1}^2}}}{\text{n1}\cos[\theta 0]+\text{n0}\sqrt{1-\frac{\sin[\theta 0]^2}{\text{n1}^2}}}+\frac{e^{-\frac{4i d\text{n1}\pi\sqrt{1-\frac{\sin[\theta 0]^2}{\text{n1}^2}}}{\lambda}}\left(\text{n2}\sqrt{1-\frac{\sin[\theta 0]^2}{\text{n1}^2}}-\text{n1}\sqrt{1-\frac{\sin[\theta 0]^2}{\text{n2}^2}}\right)}{\text{n2}\sqrt{1-\frac{\sin[\theta 0]^2}{\text{n1}^2}}+\text{n1}\sqrt{1-\frac{\sin[\theta 0]^2}{\text{n2}^2}}}\right)\left(1+\frac{e^{-\frac{4i d\text{n1}\pi\sqrt{1-\frac{\sin[\theta 0]^2}{\text{n1}^2}}}{\lambda}}\left(\text{n0}\cos[\theta 0]-\text{n1}\sqrt{1-\frac{\sin[\theta 0]^2}{\text{n1}^2}}\right)\left(\text{n1}\sqrt{1-\frac{\sin[\theta 0]^2}{\text{n1}^2}}-\text{n2}\sqrt{1-\frac{\sin[\theta 0]^2}{\text{n2}^2}}\right)}{\left(\text{n0}\cos[\theta 0]+\text{n1}\sqrt{1-\frac{\sin[\theta 0]^2}{\text{n1}^2}}\right)\left(\text{n1}\sqrt{1-\frac{\sin[\theta 0]^2}{\text{n1}^2}}+\text{n2}\sqrt{1-\frac{\sin[\theta 0]^2}{\text{n2}^2}}\right)}\right)}{\left(1+\frac{e^{-\frac{4i d\text{n1}\pi\sqrt{1-\frac{\sin[\theta 0]^2}{\text{n1}^2}}}{\lambda}}\left(\text{n1}\cos[\theta 0]-\text{n0}\sqrt{1-\frac{\sin[\theta 0]^2}{\text{n1}^2}}\right)\left(\text{n2}\sqrt{1-\frac{\sin[\theta 0]^2}{\text{n1}^2}}-\text{n1}\sqrt{1-\frac{\sin[\theta 0]^2}{\text{n2}^2}}\right)}{\left(\text{n1}\cos[\theta 0]+\text{n0}\sqrt{1-\frac{\sin[\theta 0]^2}{\text{n1}^2}}\right)\left(\text{n2}\sqrt{1-\frac{\sin[\theta 0]^2}{\text{n1}^2}}+\text{n1}\sqrt{1-\frac{\sin[\theta 0]^2}{\text{n2}^2}}\right)}\right)\left(\frac{\text{n0}\cos[\theta 0]-\text{n1}\sqrt{1-\frac{\sin[\theta 0]^2}{\text{n1}^2}}}{\text{n0}\cos[\theta 0]+\text{n1}\sqrt{1-\frac{\sin[\theta 0]^2}{\text{n1}^2}}}+\frac{e^{-\frac{4i d\text{n1}\pi\sqrt{1-\frac{\sin[\theta 0]^2}{\text{n1}^2}}}{\lambda}}\left(-1+\text{n1}^2+\text{n2}^2+\cos[2\theta 0]-2\text{n1n2}\sqrt{1-\frac{\sin[\theta 0]^2}{\text{n1}^2}}\sqrt{1-\frac{\sin[\theta 0]^2}{\text{n2}^2}}\right)}{\text{n1}^2-\text{n2}^2}\right)}$$

(* Now we assume n1 = n2, n0 = 1 to check reversion to air/substrate case. We convert $N_2^2 = \epsilon_2$ *)

n1 = n2

n0 = 1

n2 = (ϵ2)^1/2

$\sqrt{\epsilon 2}$

1

$\sqrt{\epsilon 2}$

n2

1

FullSimplify[ρ]

$$\frac{-1+\cos[2\theta 0]+2\sqrt{\epsilon 2}\cos[\theta 0]\sqrt{1-\frac{\sin[\theta 0]^2}{\epsilon 2}}}{-1+\cos[2\theta 0]-2\sqrt{\epsilon 2}\cos[\theta 0]\sqrt{1-\frac{\sin[\theta 0]^2}{\epsilon 2}}}$$

(* Now we take the difference between this and the ρ as obtained from the substrate case. We should get zero if they are the same.*)

$$\text{FullSimplify}\left[\frac{-1+\cos[2\theta 0]+2\text{n2}\cos[\theta 0]\sqrt{1-\frac{\sin[\theta 0]^2}{\text{n2}^2}}}{-1+\cos[2\theta 0]-2\text{n2}\cos[\theta 0]\sqrt{1-\frac{\sin[\theta 0]^2}{\text{n2}^2}}}-\frac{\sin[\theta 0]^2-\cos[\theta 0]\sqrt{1-\frac{\sin[\theta 0]^2}{\epsilon 2}}\sqrt{\epsilon 2}}{\sin[\theta 0]^2+\cos[\theta 0]\sqrt{1-\frac{\sin[\theta 0]^2}{\epsilon 2}}\sqrt{\epsilon 2}}\right]$$

```
0
```

(* Verified *)

Appendix D

Hamiltonian for free field of Light

The following derivation is based on a lecture on Quantum Optics by Professor Manas Mukherjee [41].

We consider an electromagnetic field without sources. In the Coulomb gauge, this reads:

$$\vec{E} = -\partial_t \vec{A} \tag{D.1}$$

$$\nabla^2 \vec{A} - \frac{1}{c^2}\partial_t^2 \vec{A} = 0 \tag{D.2}$$

The second derivative in time (Hamilton equations should only contain up to first derivatives of time) suggests that we introduce the auxiliary field in foresight.

$$\vec{\Pi} = -\epsilon_0 \vec{E} \tag{D.3}$$

Our original equations now read:

$$\partial_t \vec{A} = \frac{1}{\epsilon_0}\vec{\Pi} \tag{D.4}$$

$$\partial_t \vec{\Pi} = \epsilon_0 c^2 \nabla^2 \vec{A} \tag{D.5}$$

We now perform Fourier decomposition on the two equations. We suppose that the field is in a cubic volume of sides L with periodic boundary conditions (This should not matter as we can set $\mathrm{L} \to \infty$ at the end).

$$\vec{A}(\vec{x}) = \frac{1}{\sqrt{L^3}} \sum_{\vec{k}\in\mathcal{L}} \vec{A}_{\vec{k}} e^{i\vec{k}\cdot\vec{x}} \tag{D.6}$$

$$\vec{\Pi}(\vec{x}) = \frac{1}{\sqrt{L^3}} \sum_{\vec{k}\in\mathcal{L}} \vec{\Pi}_{\vec{k}} e^{i\vec{k}\cdot\vec{x}} \tag{D.7}$$

The above summation takes place over the set $\mathcal{L} = [\vec{k} \neq \vec{0}$ such that $k_i L = 0$ for mod$2\pi, i = x, y, z]$ which is the reciprocal lattice to the volume.

Since this is a choice of a decomposition on a set of orthogonal functions, the plane waves

$$f_{\vec{k}}(\vec{x}) = \frac{1}{\sqrt{L^3}} e^{i\vec{k}\cdot\vec{x}} \tag{D.8}$$

must satisfy

$$< f_{\vec{k}'}(\vec{x}) | f_{\vec{k}}(\vec{x}) >= \int_V \frac{1}{L^3} e^{i\vec{k}\cdot\vec{x}} e^{-i\vec{k}'\cdot\vec{x}} d^3\vec{x} = \delta_{\vec{k},\vec{k}'} \tag{D.9}$$

Thus, the Fourier coefficients of $\vec{A}$ are given by

$$\vec{A}_{\vec{k}} =< f_{\vec{k}'}(\vec{x}) | \vec{A} >= \frac{1}{\sqrt{L^3}} \int_V \vec{A}(\vec{x}) e^{-i\vec{k}\cdot\vec{x}} \tag{D.10}$$

Similarly, the Fourier coefficients of $\vec{\Pi}$ can be obtained.

As the fields $\vec{A}(\vec{x})$ and $\vec{\Pi}(\vec{x})$ are real, there is a constraint $\vec{A^*}_{\vec{k}} = \vec{A}_{-\vec{k}}$ and $\vec{\Pi^*}_{\vec{k}} = \vec{\Pi}_{-\vec{k}}$, and so these coefficients are unable to take on all possible values. To remove this constraint, we form the new variables $\vec{\alpha}_{\vec{k}} = \frac{1}{h(\vec{k})}[\epsilon_0 \omega(\vec{k}) \vec{A}_{\vec{k}} + i\vec{\Pi}_{\vec{k}}]$ where $h(\vec{k})$ is an arbitrary scalar even function that will be chosen to simplify the final expression, and

$$\omega(\vec{k}) = c|\vec{k}| \tag{D.11}$$

A second constraint was introduced right at the beginning when we decided to use the Coulomb gauge with $\vec{\nabla} \cdot \vec{A} = 0$ and $\vec{\nabla} \cdot \vec{\Pi} = 0$. This leads to the constraint $\vec{k} \cdot \vec{A}_{\vec{k}} = \vec{k} \cdot \vec{\Pi}_{\vec{k}} = 0$ which thus leads to $\vec{k} \cdot \vec{\alpha}_{\vec{k}} = 0$ for all $\vec{k} \in \mathcal{L}$, i.e. $\vec{\alpha}_{\vec{k}}$ are not independent variables yet. We thus have to define for each $\vec{k}$ two orthogonal

complex unit vectors $\hat{e}_1(\vec{k})$ and $\hat{e}_1(\vec{k})$ such that

$$\hat{e}^*_P(\vec{k}) \cdot \hat{e}_{P'}(\vec{k}) = \delta_{P,P'} \tag{D.12}$$

$$\vec{k} \cdot \hat{e}_P(\vec{k}) = 0 \tag{D.13}$$

We can now express $\vec{\alpha}_{\vec{k}} = \sum_{P=1,2} \alpha_{\vec{k},P} \hat{e}_P(\vec{k})$ where the Mode Amplitudes $\alpha_{\vec{k},P}$ are the independent variables that we want.

Putting everything back together, it is convenient to choose $h(\vec{k}) = \sqrt{2\epsilon_0 h_0 \omega(\vec{k})}$ where h_0 is an arbitrary constant of dimension [energy $\times$ time]. We thus obtain

$$\vec{A}(\vec{x}) = \sum_{\vec{k}\in\mathcal{L}} \sum_{P=1,2} \alpha_{\vec{k},P} \vec{A}_{\vec{k},P}(\vec{x}) + c.c. \tag{D.14}$$

$$\vec{\Pi}(\vec{x}) = \sum_{\vec{k}\in\mathcal{L}} \sum_{P=1,2} (-i\epsilon_0 \omega(\vec{k})) \alpha_{\vec{k},P} \vec{A}_{\vec{k},P}(\vec{x}) + c.c. \tag{D.15}$$

where

$$\vec{A}_{\vec{k},P}(\vec{x}) = \sqrt{\frac{h_0}{2L^3\epsilon_0\omega(\vec{k})}} \hat{e}_P(\vec{k}) e^{i\vec{k}\cdot\vec{x}} \tag{D.16}$$

Re-expressing the independent mode amplitudes as functions of the fields, we get

$$\alpha_{\vec{k},P} = \frac{1}{h_0} \int_V \vec{A^*}_{\vec{k},P}(\vec{x}) [\epsilon_0 \omega(\vec{k}) \vec{A}(\vec{x}) + i\vec{\Pi}(\vec{x})] d^3\vec{x} \tag{D.17}$$

Differentiating it with respect to time, we get

$$\dot{\alpha}_{\vec{k},P} = \frac{1}{h_0} \int_V \vec{A^*}_{\vec{k},P}(\vec{x}) [\epsilon_0 \omega(\vec{k}) \partial_t \vec{A}(\vec{x}) + i\partial_t \vec{\Pi}(\vec{x})] d^3\vec{x} \tag{D.18}$$

Substituting (D.4) and (D.5), we get

$$\dot{\alpha}_{\vec{k},P} = \frac{1}{h_0}(-i\omega(\vec{k})) \int_V \vec{A^*}_{\vec{k},P}(\vec{x}) [i\vec{\Pi}(\vec{x}) + \epsilon_0 \omega(\vec{k}) \vec{A}(\vec{x})] d^3\vec{x} \tag{D.19}$$

Using Green's theorem [$\int_V (\phi\nabla^2\psi - \psi\nabla^2\phi) d^3\vec{x} = \int_S (\phi\vec{\nabla}\psi - \psi\vec{\nabla}\phi)\cdot d\vec{\sigma}$], the whole

expression simplifies into

$$\dot{\alpha}_{\vec{k},P} = -i\omega(\vec{k})\alpha_{\vec{k},P} \tag{D.20}$$

which leads to the well-known solution

$$\alpha_{\vec{k},P}(t) = \alpha_{\vec{k},P}(0)e^{-i\omega(\vec{k})t} \tag{D.21}$$

where we can see that there is no mode-coupling.

$\alpha_{\vec{k},P}(t)$ is in general complex, and so we can split it and rewrite as

$$\alpha_{\vec{k},P}(t) = \frac{\omega(\vec{k})q_{\vec{k},P} + ip_{\vec{k},P}}{\sqrt{2h_0\omega(\vec{k})}} \tag{D.22}$$

Re-inserting into (D.20), we obtain the evolution

$$\dot{q}_{\vec{k},P} = p_{\vec{k},P} \tag{D.23}$$

$$\dot{p}_{\vec{k},P} = -\omega(\vec{k})^2 q_{\vec{k},P} \tag{D.24}$$

which are immediately recognizable as the Hamilton equations for the hamiltonian operator of the harmonic oscillator

$$\sum_{\vec{k}\in\mathcal{L}} \sum_{P=1,2} H_{\vec{k},P} \tag{D.25}$$

where

$$H_{\vec{k},P} = \frac{p^2_{\vec{k},P} + \omega(\vec{k})^2 q^2_{\vec{k},P}}{2} \tag{D.26}$$

We have thus shown that a free field of light can be described as a collection of independent harmonic oscillators.

Appendix E

Error analysis for Kramers-Kronig transformation (Matlab code)

A set of "perfect" ϵ_1 and ϵ_2 as a function of photon energy is created using the Lorentz model. Data values are then extracted at suitable intervals (depending on the desired data point density and energy range). The Kramers-Kronig transformation is then used to obtain the transformed ϵ_2 from the analytical ϵ_1 values, and the transformed ϵ_1 from the analytical ϵ_2 values. To compare the results, the absolute and percentage error is taken at each data point and the errors plotted out.

E.1 100 data points, 13.2eV range

```
clc;

clear all;

close all;
```

Creating the perfect epsilons

```
pts = 100;

w = (10^15*linspace(0,20,pts)');

dw = (max(w)-min(w))/pts;

ev = 1.0546*10^-34 * w'/(1.6*10^-19);

gamma = 1.2*10^15;

A = 1.6*10^32;

w0 = 6.08*10^15;

e1perf = 1+A*(w0^2-w.^2)./((w0^2-w.^2).^2+(gamma*w).^2);

e2perf = A*(gamma*w)./((w0^2-w.^2).^2+(gamma*w).^2);

e1 = zeros(pts,1);

e2 = zeros(pts,1);
```

The KK

```
for i=1:pts
for j=1:i-1
e1(i) = e1(i)+2/pi*(w(j)*e2perf(j))/(w(j)^2-w(i)^2)*dw;
end
for j=i+1:pts
e1(i) = e1(i)+2/pi*(w(j)*e2perf(j))/(w(j)^2-w(i)^2)*dw;
end
end
for i=1:pts
for j=1:i-1
e2(i) = e2(i)-2*w(i)/pi*(e1perf(j)-1)/(w(j)^2-w(i)^2)*dw;
end
for j=i+1:pts
e2(i) = e2(i)-2*w(i)/pi*(e1perf(j)-1)/(w(j)^2-w(i)^2)*dw;
end
end
```

```
e1 = e1+1;
```

The errors

```
e1err = (e1-e1perf);
e2err = (e2-e2perf);
percente1err = (e1-e1perf)*100./(e1perf);
percente2err = (e2-e2perf)*100./(e2perf);
```


E.2 Comparing 6.5eV range to 20eV range with constant data point density of ≈ 150 points per eV

The parameter 'runs' can be adjusted from 1 to 21 to change the range from 10×10^{15} rad/s (6.5 eV) to 30×10^{15} rad/s (20 eV).

```
clc;
clear all;
close all;
runs = 21;
abs_errormatrix = zeros(50*runs,3*runs);
```

```
for k = 1:runs
```

Creating the perfect epsilons

```
pts = 900 +k*100;
w = (10^15*linspace(0,9+k,pts)');
dw = (max(w)-min(w))/pts;
ev = 1.0546*10^-34 * w'/(1.6*10^-19);
gamma = 1.2*10^15;
A = 1.6*10^32;
w0 = 6.08*10^15;
e1perf = 1+A*(w0^2-w.^2)./((w0^2-w.^2).^2+(gamma*w).^2);
e2perf = A*(gamma*w)./((w0^2-w.^2).^2+(gamma*w).^2);
e1 = zeros(pts,1);
e2 = zeros(pts,1);
```

The KK

```
for i=1:pts
```

```
for j=1:i-1
e1(i) = e1(i)+2/pi*(w(j)*e2perf(j))/(w(j)^2-w(i)^2)*dw;
end
for j=i+1:pts
e1(i) = e1(i)+2/pi*(w(j)*e2perf(j))/(w(j)^2-w(i)^2)*dw;
end
end
for i=1:pts
for j=1:i-1
e2(i) = e2(i)-2*w(i)/pi*(e1perf(j)-1)/(w(j)^2-w(i)^2)*dw;
end
for j=i+1:pts
e2(i) = e2(i)-2*w(i)/pi*(e1perf(j)-1)/(w(j)^2-w(i)^2)*dw;
end
end
e1 = e1+1;
```

The errors

```
perc_errormatrix(1:pts,3*k-2) = ev;

perc_errormatrix(1:pts,3*k-1) = abs((e1-e1perf)*100./e1perf);

perc_errormatrix(1:pts,3*k) = abs((e2-e2perf)*100./e2perf);


abs_errormatrix(1:pts,3*k-2) = ev;

abs_errormatrix(1:pts,3*k-1) = abs(e1-e1perf);

abs_errormatrix(1:pts,3*k) = abs(e2-e2perf);


end
```

E.3 Comparing 50 data points to 1000 data points, 13.2eV range

The parameter 'runs' can be adjusted from 1 to 20 to change the number of data points from 50 to 1000.

```
clc;

clear all;

close all;
```

```
runs = 20;
perc_errormatrix = zeros(50*runs,3*runs);
abs_errormatrix = zeros(50*runs,3*runs);
for k = 1:runs
```

creating the perfect epsilons

```
pts = k*50;
w = (10^15*linspace(0,20,pts)');
dw = (max(w)-min(w))/pts;
ev = 1.0546*10^-34 * w'/(1.6*10^-19);
gamma = 1.2*10^15;
A = 1.6*10^32;
w0 = 6.08*10^15;
e1perf = 1+A*(w0^2-w.^2)./((w0^2-w.^2).^2+(gamma*w).^2);
e2perf = A*(gamma*w)./((w0^2-w.^2).^2+(gamma*w).^2);
e1 = zeros(pts,1);
e2 = zeros(pts,1);
```

The KK

```
for i=1:pts
for j=1:i-1
e1(i) = e1(i)+2/pi*(w(j)*e2perf(j))/(w(j)^2-w(i)^2)*dw;
end
for j=i+1:pts
e1(i) = e1(i)+2/pi*(w(j)*e2perf(j))/(w(j)^2-w(i)^2)*dw;
end
end
for i=1:pts
for j=1:i-1
e2(i) = e2(i)-2*w(i)/pi*(e1perf(j)-1)/(w(j)^2-w(i)^2)*dw;
end
for j=i+1:pts
e2(i) = e2(i)-2*w(i)/pi*(e1perf(j)-1)/(w(j)^2-w(i)^2)*dw;
end
end
```

```
e1 = e1+1;
```

The errors

```
perc_errormatrix(1:pts,3*k-2) = ev;

perc_errormatrix(1:pts,3*k-1) = abs((e1-e1perf)*100./e1perf);

perc_errormatrix(1:pts,3*k) = abs((e2-e2perf)*100./e2perf);


abs_errormatrix(1:pts,3*k-2) = ev;

abs_errormatrix(1:pts,3*k-1) = abs(e1-e1perf);

abs_errormatrix(1:pts,3*k) = abs(e2-e2perf);


end
```

Appendix F

Manual fitting of the Lorentz model to experimental data (Matlab code)

The code imports raw experimental Ψ and Δ values for film-on-substrate (data2.dat) and for substrate (data.dat). It then matches and extracts the data such that for each energy value, we have the substrate optical constants, and Ψ/Δ values for 2 different incident angles for the film-on-substrate data set. This is only done for robustness and future expansion since only 1 set of Ψ/Δ values is needed here.

A model with 3 Lorentzians is created, with its parameters inserted by hand, and a "fitted" ρ is calculated using it together with the substrate data. It is then compared with the experimental ρ for film-on-substrate.

```
clc;
clear all;
close all;

%%importing from data.dat into result matrix
substrate = [];
fid=fopen('data.dat');
while 1
tline = fgetl(fid);
if ~ischar(tline), break, end
celldata = textscan(tline,'%f %f %f %f %f %f');
matdata = cell2mat(celldata);
% match fails for text lines, textscan returns empty cells
substrate = [substrate ; matdata];
end
fclose(fid);

%%importing from data2.dat into result2 matrix
```

```
layers = [];
fid2=fopen('data2.dat');
while 1
tline2 = fgetl(fid2);
if ~ischar(tline2), break, end
celldata2 = textscan(tline2,'%f %f %f %f %f %f');
matdata2 = cell2mat(celldata2);
% match fails for text lines, textscan returns empty cells
layers = [layers ; matdata2];
end
fclose(fid2);

%%specify your thetas for multilayer data here
theta1=40;
theta2=70;
%%extracts rows with specified theta
layers_fulltheta1_index=find(layers(:,2)==theta1);
layers_fulltheta2_index=find(layers(:,2)==theta2);
```

```
%%match eV
layers_fulltheta1_theta=layers(layers_fulltheta1_index,:);
layers_fulltheta2_theta=layers(layers_fulltheta2_index,:);
[layers_matched_thetas_ev,layers_matchedtheta1_index,layers_matchedtheta2_index]=
intersect(layers_fulltheta1_theta(:,1),layers_fulltheta2_theta(:,1));
%%consolidating multilayer data: [eV   theta1   layers_theta1_psi
   layers_theta1_delta   theta2   layers_theta2_psi  layers_theta2_delta
layers_data = [];
layers_data(:,1)=layers_matched_thetas_ev;
layers_data(:,2)=layers_fulltheta1_theta(layers_matchedtheta1_index,2);
layers_data(:,3)=layers_fulltheta1_theta(layers_matchedtheta1_index,3);
layers_data(:,4)=layers_fulltheta1_theta(layers_matchedtheta1_index,4);
layers_data(:,5)=layers_fulltheta2_theta(layers_matchedtheta2_index,2);
layers_data(:,6)=layers_fulltheta2_theta(layers_matchedtheta2_index,3);
layers_data(:,7)=layers_fulltheta2_theta(layers_matchedtheta2_index,4);

%%specify your theta for substrate here
theta_sub=50;
```

```
%%extracts rows with specified theta
substrate_fulltheta_index=find(substrate(:,2)==theta_sub);
substrate_fulltheta_ev=substrate(substrate_fulltheta_index,1);
%%converting from psi/delta to epsilon 1 and 2
rho_substrate=tand(substrate(substrate_fulltheta_index,3)).*exp(1i.*substrate(substrate_fulltheta_index,4)./180.*pi);
epsilon_substrate=(sind(theta_sub)^2)*(1+(tand(theta_sub)^2).*((1.-rho_substrate)./(1.+rho_substrate)).^2);
e1perf_substrate=real(epsilon_substrate);
e2perf_substrate=-imag(epsilon_substrate);
%%consolidating substrate data
substrate_data = [];
substrate_data(:,1)=substrate_fulltheta_ev;
substrate_data(:,2)=e1perf_substrate;
substrate_data(:,3)=e2perf_substrate;
substrate_data(:,4)=rho_substrate;

%%Final matching between multilayer data and substrate data
[matched_ev_final,matched_layers_index,matched_substrate_index]=intersect(layers_data(:,1),substrate_data(:,1));
```

```
%{consolidating: [en   theta1   layers_theta1_psi
layers_theta1_delta   rho(theta1)   theta2
layers_theta2_psi  layers_theta2_delta
rho(theta2)   substrate_e1   substrate_e2   n_substrate   rho_substrate]
%}
matched_data = [];
matched_data(:,1)=matched_ev_final.*((1.6*10^-19)/(1.0546*10^-34));
matched_data(:,2)=layers_data(matched_layers_index,2)./180*pi;
matched_data(:,3)=layers_data(matched_layers_index,3)./180*pi;
matched_data(:,4)=layers_data(matched_layers_index,4)./180*pi;
matched_data(:,5)=(tan(matched_data(:,3)).*exp(1i*matched_data(:,4)));
matched_data(:,6)=layers_data(matched_layers_index,5)./180*pi;
matched_data(:,7)=layers_data(matched_layers_index,6)./180*pi;
matched_data(:,8)=layers_data(matched_layers_index,7)./180*pi;
matched_data(:,9)=(tan(-matched_data(:,7)).*exp(1i*matched_data(:,8)));
matched_data(:,10)=substrate_data(matched_substrate_index,2);
matched_data(:,11)=substrate_data(matched_substrate_index,3);
matched_data(:,12)=sqrt(matched_data(:,10)-1i*matched_data(:,11));
```

```
matched_data(:,13)=substrate_data(matched_substrate_index,4);


[m,p]=size(matched_data);

%%Now to guess for e1 and e2
```

creating the guessed epsilon 1 and 2

```
pts = m;
w = matched_data(:,1);
dw = (max(w)-min(w))/pts;


w01 = 2.35*1.6*10^-19/(1.055*10^-34);
gamma1 = 0.5*(1.6*10^-19)/(1.055*10^-34);
A1 = 2*10^32;


w02 = 3.3*1.6*10^-19/(1.055*10^-34);
gamma2 = 0.5*1.6*10^-19/(1.055*10^-34);
A2 = 2*10^32;
```

```
w03 = 4.05*1.6*10^-19/(1.055*10^-34);
gamma3 = 0.5*1.6*10^-19/(1.055*10^-34);
A3 =2*10^32;

e1perf = 1+A1*(w01^2-w.^2)./((w01^2-w.^2).^2+(gamma1*w).^2) +
A2*(w02^2-w.^2)./((w02^2-w.^2).^2+(gamma2*w).^2) +
A3*(w03^2-w.^2)./((w03^2-w.^2).^2+(gamma3*w).^2);
e2perf = A1*(gamma1*w)./((w01^2-w.^2).^2+(gamma1*w).^2) +
A2*(gamma2*w)./((w02^2-w.^2).^2+(gamma2*w).^2) +
A3*(gamma3*w)./((w03^2-w.^2).^2+(gamma3*w).^2);
n1=sqrt(e1perf - 1i*e2perf);

%%Now we calculate psi and delta from guessed e1e2 and substrate e1e2

n0=1;
d=14*10^-10;
theta0=matched_data(:,2);
```

```
lambda=(3*10^8).*(2*pi)./matched_data(:,1);
n2=matched_data(:,12);
%n2=1;

rho=((n1.*cos(theta0)+(-1).*n0.*(1+(-1).*n1.^(-2).*sin(theta0).^2).^( ...
1/2)).*(n1.*cos(theta0)+n0.*(1+(-1).*n1.^(-2).*sin(theta0).^2).^( ...
1/2)).^(-1)+exp(1).^((sqrt(-1)*(-4)).*d.*lambda.^(-1).*n1.*pi.*(1+ ...
(-1).*n1.^(-2).*sin(theta0).^2).^(1/2)).*(n2.*(1+(-1).*n1.^(-2).* ...
sin(theta0).^2).^(1/2)+(-1).*n1.*(1+(-1).*n2.^(-2).*sin(theta0) ...
.^2).^(1/2)).*(n2.*(1+(-1).*n1.^(-2).*sin(theta0).^2).^(1/2)+n1.*( ...
1+(-1).*n2.^(-2).*sin(theta0).^2).^(1/2)).^(-1)).*(1+exp(1).^(( ...
sqrt(-1)*(-4)).*d.*lambda.^(-1).*n1.*pi.*(1+(-1).*n1.^(-2).*sin( ...
theta0).^2).^(1/2)).*(n1.*cos(theta0)+(-1).*n0.*(1+(-1).*n1.^(-2) ...
.*sin(theta0).^2).^(1/2)).*(n1.*cos(theta0)+n0.*(1+(-1).*n1.^(-2) ...
.*sin(theta0).^2).^(1/2)).^(-1).*(n2.*(1+(-1).*n1.^(-2).*sin( ...
theta0).^2).^(1/2)+(-1).*n1.*(1+(-1).*n2.^(-2).*sin(theta0).^2).^( ...
1/2)).*(n2.*(1+(-1).*n1.^(-2).*sin(theta0).^2).^(1/2)+n1.*(1+(-1) ...
.*n2.^(-2).*sin(theta0).^2).^(1/2)).^(-1)).^(-1).*(1+exp(1).^(( ...
```

```
sqrt(-1)*(-4)).*d.*lambda.^(-1).*n1.*pi.*(1+(-1).*n1.^(-2).*sin( ...
theta0).^2).^(1/2)).*(n0.*cos(theta0)+(-1).*n1.*(1+(-1).*n1.^(-2) ...
.*sin(theta0).^2).^(1/2)).*(n0.*cos(theta0)+n1.*(1+(-1).*n1.^(-2) ...
.*sin(theta0).^2).^(1/2)).^(-1).*(n1.*(1+(-1).*n1.^(-2).*sin( ...
theta0).^2).^(1/2)+(-1).*n2.*(1+(-1).*n2.^(-2).*sin(theta0).^2).^( ...
1/2)).*(n1.*(1+(-1).*n1.^(-2).*sin(theta0).^2).^(1/2)+n2.*(1+(-1) ...
.*n2.^(-2).*sin(theta0).^2).^(1/2)).^(-1)).*((n0.*cos(theta0)+(-1) ...
.*n1.*(1+(-1).*n1.^(-2).*sin(theta0).^2).^(1/2)).*(n0.*cos(theta0) ...
+n1.*(1+(-1).*n1.^(-2).*sin(theta0).^2).^(1/2)).^(-1)+exp(1).^(( ...
sqrt(-1)*(-4)).*d.*lambda.^(-1).*n1.*pi.*(1+(-1).*n1.^(-2).*sin( ...
theta0).^2).^(1/2)).*(n1.^2+(-1).*n2.^2).^(-1).*((-1)+n1.^2+n2.^2+ ...
cos(2.*theta0)+(-2).*n1.*n2.*(1+(-1).*n1.^(-2).*sin(theta0).^2).^( ...
1/2).*(1+(-1).*n2.^(-2).*sin(theta0).^2).^(1/2))).^(-1);

%%Now comparing guessed rho with experimental rho
%{
figure;plot(matched_data(:,1).*(1.055*10^-34)./(1.6*10^-19),real(rho),
matched_data(:,1).*(1.055*10^-34)./(1.6*10^-19),imag(rho))
```

```
title('Fitted Real and Imaginary \rho');
%axis([0 5 -0.4 0.2]);
xlabel('Photon energy (eV)');
ylabel('\rho');
legend('Re(\rho)','Im(\rho)');
%}
```

Appendix G

Analysis of fitting attempts for MoS_2 bilayer on STO using 3 layer optical model and 3-Lorentzian model

An example of a fitted curve is shown in Fig. G.1. The fitting parameters listed in

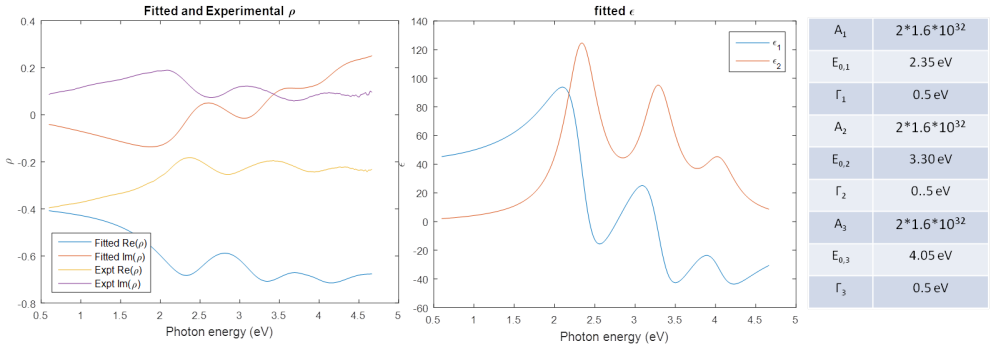

Fig. G.1. Example of fitting attempt of MoS_2 bilayer (1)

Fig. G.1 correspond to the equations (G.1) and (G.2) where E denotes the incident photon energy.

$$\epsilon_1 = 1 + \sum_k A_k \frac{(E^2 - E_{0,k}^2)}{(E^2 - E_{0,k}^2)^2 + \Gamma_k^2 E^2} \tag{G.1}$$

$$\epsilon_2 = \sum_k A_k \frac{\Gamma_k E}{(E^2 - E_{0,k}^2)^2 + \Gamma_k^2 E^2} \tag{G.2}$$

Several factors point to the insufficiency of the models used rather than poor choice of fitting parameters as the cause of failure:

- Any lorentzian amplitude ratio A_i that can achieve the prominent peaks visible in the experimental $\mathrm{Re}(\rho)$ and $\mathrm{Im}(\rho)$ leads to ϵ values that are in the hundreds (Expected values are on the order 0 to 20 for monolayer MoS_2 on STO substrate [16]).

- The general shape of the fitted ρ is wrong (Fig. G.2). The shapes imply that our model requires a phase change to "flip" everything, suggesting that a 4 layer optical model might be more suitable.

- Reducing the amplitudes A_i to obtain ϵ values of the correct order of magnitude reveals a prominent structure around 3.8 eV (Fig. G.3), which is due to the substrate (Section 3.4.1)

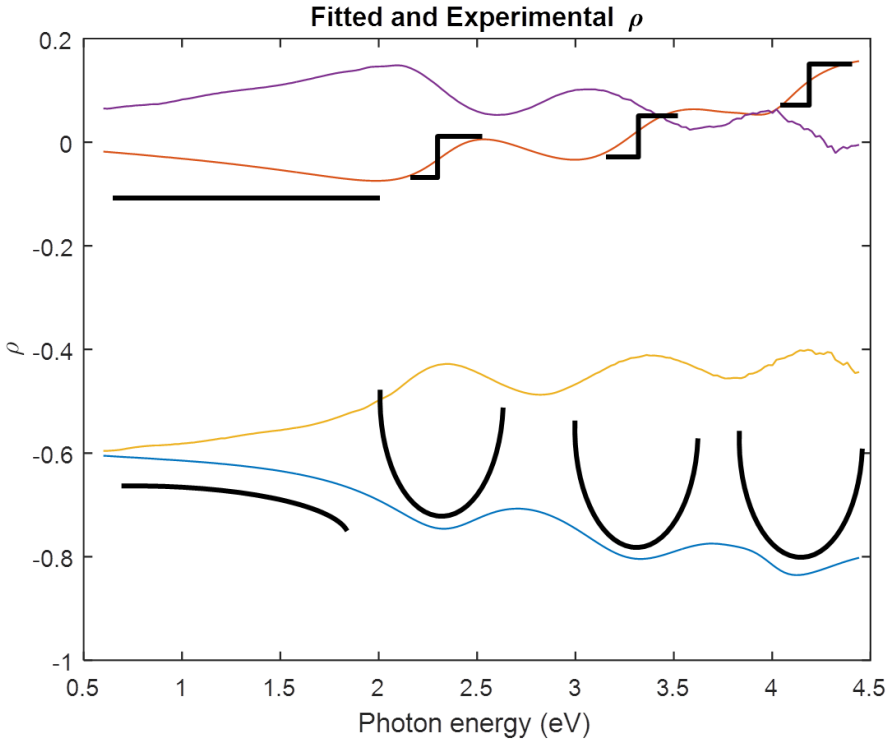

Fig. G.2. General shape of fitted ρ using 3 optical layer, 3 lorentzian model

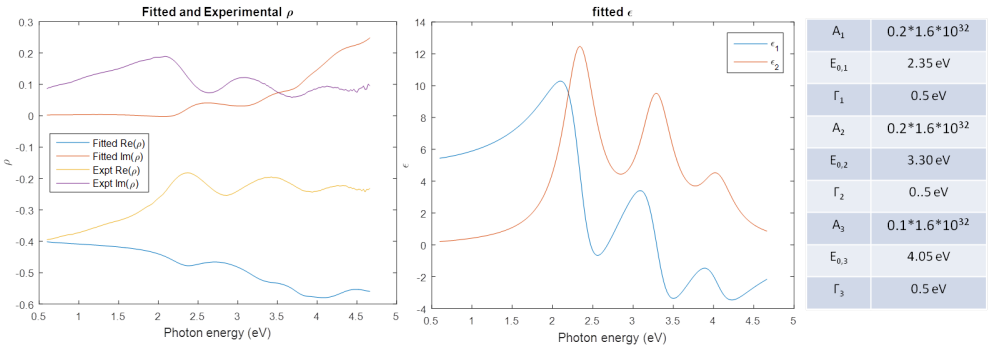

A_1	$0.2*1.6*10^{32}$
$E_{0,1}$	2.35 eV
Γ_1	0.5 eV
A_2	$0.2*1.6*10^{32}$
$E_{0,2}$	3.30 eV
Γ_2	0..5 eV
A_3	$0.1*1.6*10^{32}$
$E_{0,3}$	4.05 eV
Γ_3	0.5 eV

Fig. G.3. Example of fitting attempt of MoS_2 bilayer (2). Note the structure at 3.8 eV that is due to the substrate

Taken together, the observations listed above suggest that our 3 layer optical model (air-film-substrate) is insufficient, and an interface layer between the film and the substrate is needed. This might provide the phase change required to "flip" the curves, and could also provide the screening effect that washes out the substrate structure at 3.8 eV.